Crystallinity and Albedo: In-situ VNIR Analysis of Glassy lava flow Surfaces at Jordan Craters, OR

A Dissertation
Presented in Partial Fulfillment of the Requirements for the
Degree of Master of Science
with a
Major in Geology
in the
College of Graduate Studies
University of Idaho
by
Adrianne Reeder

Major Professor: Erika Rader, Ph.D.
Committee Members: Leslie Baker, Ph.D.; Thomas Williams, Ph.D.
Department Administrator: Leslie Baker, Ph. D.

December 2020

Authorization to Submit Thesis

This thesis of Adrianne Reeder submitted for the degree of Master of Science with a Major in Geology and titled " Crystallinity and Albedo: In-situ VNIR Analysis of Glassy lava flow Surfaces at Jordan Craters, OR," has been reviewed in final form. Permission, as indicated by the signatures and dates below, is now granted to submit final copies to the College of Graduate Studies for approval.

Major Professor: _____ Date: _____
Erika Rader, Ph.D.

Committee Members: _____ Date: _____
Leslie Baker, Ph.D.

_____ Date: _____
Thomas Williams, Ph.D.

Department Administrator: _____ Date: _____
Leslie Baker, Ph.D.

Abstract

We present an in-situ analysis of the albedo of Visible Near Infrared (VNIR) and the petrologic texture of the surface of a glassy lava flow at Jordan Craters, OR. 10 of our collected samples, from the surface and vent of our flow, had very low reflectance in the VNIR range 0.02 – 0.04 and textures of mostly glass and phenocrysts of olivine and plagioclase. These dark samples were rapidly quenched morphologies, like spatter and scoria. Samples that had brighter VNIR (33% of samples) and had defined absorption bands at 500nm, 1500nm, 1900nm, and 2100nm also had devitrification, alteration, or higher crystal content, and were collected along the margins of the flow. Alteration was identified through the presence of specific absorption bands, e.g. 1900nm, while devitrification and higher crystal content were differentiated based on the depth of the absorption bands, with higher crystal content having the more well-defined absorption bands. We attribute these variations, alteration and devitrification, to the presence of water both during emplacement and post-cooling. A ~0.03 change in albedo that correlated to a range of 28% to 81% glass content across the flow was most clear from the in-situ measurements but was also broadly detectable from satellite ASTER data. Our findings indicate that VNIR can be used to identify variations in petrologic texture across glassy basaltic lava flows. In settings where in-situ study is not possible, such as on Mars, satellite data may give insight to where quenched basalts occur. This has implications for estimating the distribution of ancient water or ice on Mars and will allow for the better identification of locations for in-situ study by rovers for looking for evidence of ancient life.

Acknowledgements

I would like to thank NASA (80NSSC18K1518) for support. I would like to thank the Bureau of Land Management, Vale District Office for giving us access to Jordan Craters. I would like to thank Aly Doloughan and Kevin Cerna for their assistance.

Dedication

I would like to thank my family for supporting me, my friends, Shannon and Thor for listening to me and giving me courage. I'd like to thank Daniel for the laughs when I needed them.

Table of Contents

List of Tables

List of Figures

Section 1: Introduction

During the Hesperian Period of Mars, a warming CO2-rich atmosphere could have been maintained by volcanic recycling (McKay et al., 1992; Chassefière et al., 2013). If the temperature was above freezing, then it is possible that life could have flourished under these conditions (McKay and Stocker 1989; Postawko and Kuhn, 1986; McKay and Davis, 1991; McKay et al. 1992). However, Mars would have begun to cool due to the solidification of its molten-iron core, thus limiting how much microbial life could have survived as more and more liquid water was removed from the surface (Carr, 1996; Cousins and Crawford, 2011). Searching for evidence of possible past life on Mars is rife with challenges. All study thus far has been done remotely, because sending humans to Mars is not yet feasible, and by either a rover or a satellite, which greatly limits the types of data that can be gathered (Dyar and Schaefer, 2004; Young et al 2005; Navarro-Gonzalez et al.; 2006, Hecker et al.; 2010).

Places that were once ancient water sources are considered by many to have housed ancient life, which makes them the best sites for searching for evidence of life on Mars (McKay et al. 1992; Fisk and Giovannoni, 1999). On Mars, one hypothesis is that ancient water sources could have been produced and protected by ice/lava interactions (Cousins and Crawford, 2011). On Earth, ice/lava interactions create hydrothermal systems that promote and protect microbial life, if this holds true on Mars, then these sites are ideal for the search for evidence of life on Mars (Cousins and Crawford, 2011; Martin et al., 2008; Jakobsson and Gudmundsson, 2008; Boston et al., 1992; Farmer, 1996; Gulick, 1998; Payne and Farmer, 2001; Hovius et al., 2008). Ice rapidly quenches lava, producing zones of volcanic glass and on Earth these glass rich zones have housed endolithic organisms, or organisms that penetrate and live in stone. On Mars evidence of this same phenomena could be preserved to this day (Cousins and Crawford, 2011). Glass from impact sites has also been known to preserve these biosignatures (Howard et al.; 2013; Schultz et al., 2014) If theses biosignatures can be identified then these glass rich zones both those caused by lava-water interactions and impact zones, can hold evidence for past life (Cannon and Mustard, 2015).

Identifying Water on Mars:

Identifying areas of lava/water interactions has previously been done through either the visual identification of surface structures such as rootless cones or by identifying substantial mineral alteration through spectral data like VNIR (Greely and Fagents, 2001; Haskin et al., 2005; Bruno et al., 2006; Fagents and Thordarson, 2007; Ehlmann et al., 2011; Hamilton et al. 2011). Hydrous alteration occurs as water chemically breaks down and weathers the surface of the flow to create minerals that are more stable at low temperatures. Hydrous alteration is dependent on the presence of

water and it produces new minerals on the surface like goethite or smectite some of which can be identified with VNIR (Greenberger et al., 2012; Horgan et al., 2017; Yant et al., 2018).

Remote compositional data sets are produced using the Compact Reconnaissance Imaging Spectrometer for Mars (CRISM) to look for evidence of hydrous alteration (Murchie et al 2009; Brown et al. 2010). CRISM is sensitive to light within the wavelengths of 1 to 4 microns which displays the unique spectral signatures of alteration minerals, such as smectite and kaolinite, making it ideal for identifying them on the Martian surface (Brown and Storrie-Lombardi, 2006; Brown et al., 2008a). The presence of hydrous alteration on Mars is well documented (Allen et al., 1981; Bell, 2008; Farrand et al., 2016b, Sætre, 2019). The Spirit and Opportunity rovers found evidence of the presence of hematite, Al- and Fe-smectites, and hydrated Mg-sulfates on Mars (Farrand et al., 2016b).

We know on Earth that these hydrous minerals won't form if the interaction with water is brief or seasonal (Fagents and Thordarsen, 2007). Rootless cones, a formation that can be used to identify lava-water interactions, will not form if the ratio of lava to water is too low (Fagents and Thordarsen, 2007; Boreham et al., 2018). Thus, looking solely for the presence of hydrous alteration minerals or rootless cones may exclude a large proportion of water-lava interactions.

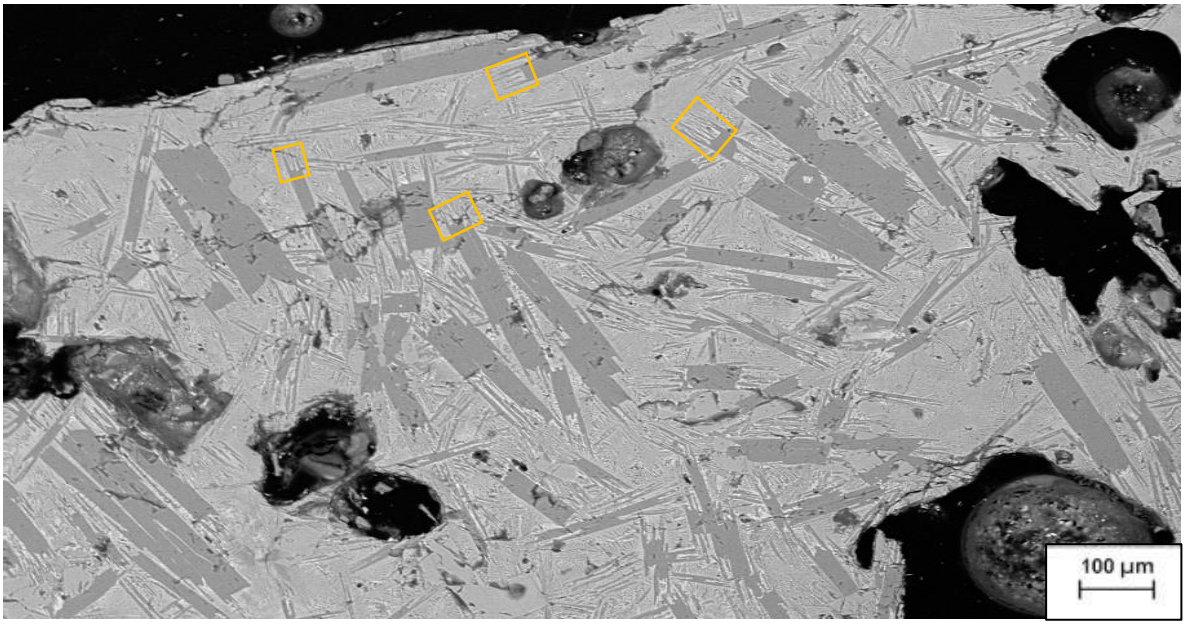

Figure 1.1: A BSE image taken of a spatter sample from Jordan Craters flow. The image shows dark plagioclase crystals with tails some outlined in orange for clarity, called swallow tail plagioclase. These are indicative of rapid quenching.

An indicator that more universally correlates with the rapid cooling that results from water/lava interactions is a mineralogical 'quench texture' (Figure 1.1). Rapidly quenched basalt has fewer and smaller crystals that are encapsulated in a glassy matrix when compared with basalts that cooled more

slowly via contact cooling and convection with the atmosphere (Szramek et al. 2006; Cashman, 1993; Wall et al, 2014). Locating these glass-rich quench textures on a flow surface would identify potential locations of ancient water (Hovius et al., 2008; Hamilton et al. 2011). However, a single basalt flow can be texturally complex and heterogeneous depending on the conditions of the eruption, which adds another layer of difficulty in identifying quench textures using remote sensing data, since the entire flow will not have the same texture and textures can vary from surface to surface.

Textural Complexities in Basalts:

Examining the petrologic texture of glassy lava can help us distinguish if water was present on a planet's surface during or after eruption. The mineralogic texture of a basalt can be used to infer the physical and chemical conditions of the magma system as well as the conditions under which the basalt erupted (Lofgren, 1974; Ginibre et al., 2002; Bennett et al. 2019). Texture refers to the phases present in the rock, the crystal size distribution and the shape of the minerals. Each of these components can reveal details about the petrogenesis of the sample (Nelson and Montana, 1992; Pan and Batiza, 2003; Ustunisik et al., 2014). There are four stages in the petrogenesis of a basalt that will influence the final texture.

These stages are:

1) Conditions in the magma chamber (Bindeman, 2003; Cabane et al., 2005; Pupier et al. 2008)

2) Eruption phase (Cashman, 1993; Szramek et al., 2010; Wall et al., 2014)

3) Emplacement (Quench Textures) (Jafri and Charan, 1992; Carli et al. 2015; Bennett et al., 2019)

4) Post-cooling (Michalski et al. 2006; Horgan et al., 2017; Yant et al., 2018)

Each of these stages is part of the solidification process of the lava and represents a key portion of the thermal history of the cooled lava. Because of this, each stage has an effect on the texture of the basalt, and not all of these stages will have the same effect on the entire flow, particularly the last two stages. The first stage, the conditions within the magma chamber, such as the temperature of the chamber and the mineral assemblage within it, represents the beginning of the thermal history of the magma (Pichavant et al., 2002; Donato et al., 2006). The more slowly a magma cools the more it will favor the growth of existing crystals over the formation of new crystals (Cashman and Marsh, 1988; Cashman, 1993). So slower cooling rates in the chamber will have, overall, larger crystals that are less densely spaced when compared to magmas with a faster cooling rate (Bindeman, 2003; Cabane et al., 2005; Pupier et al., 2008). For simple magma systems, a single eruption will begin with the

crystal size and distribution seen in the chamber. However, in the case of more complex systems, magma mixing can abruptly change conditions in the chamber and result in eruptive material that is distinct from the chamber. (Coombs et al., 2000; Salisbury et al., 2008). Regardless of this, the erupting material's texture will then be further affected during the second stage.

When external water interacts with lava during the second stage, eruption phase, the lava is cooled more rapidly, producing differing eruption styles and textures. Eruptions styles that interact with ground or surface water (also known as phreatomagmatic) will have rapidly cooled eruptive material due to the presence of water, which based on the same principles of cooling rate affecting crystal size and distribution, will result in less crystal growth and a higher glass content (at >40% groundmass crystallinity), when compared to Strombolian or Plinian style eruptions, which have a groundmass crystallinity of 30-40% (Cashman, 1993; Szramek et al., 2010; Wall et al. 2014).

The third stage is emplacement, which is defined by how and where a lava is erupted and cooled. Different emplacement styles will have their own unique thermal histories and cooling rates, which can vary greatly across a single flow, depending on the environmental conditions of the surrounding area, such as the temperature and presence of water. As lava flows across a surface, it will begin to cool, the speed of which will affect the morphology of the resulting flow, producing flows like pahoehoe or a'a, depending on the cooling rate and the resulting viscosity changes (Sato, 1995). These types of flows will have different surface and petrologic textures, with a'a flows having a rougher surface texture and more glass due to rapid cooling when compared to the smooth surfaces of pahoehoe (Hon et al., 1994; Sato, 1995; Cashman et al., 1999). Lava flowing in open channels will cool more quickly than lava flowing through insulated tubes, which will further diversify the texture of the basalt across a flow, as lavas that cool more rapidly will have more microlites and glass when compared to slower cooling basalts that will have larger phenocrysts that are more spaced out (Keszthelyi, 1995; Cashman et al., 1999). Lava emplaced near the vents can be thrown into the air and rapidly quenched into scoria, or partially quenched and land as spatter (Valentine et al., 2007; Cimarelli et al. 2010). Lava that is emplaced into water will be rapidly quenched, thus resulting in a glassier texture than lavas that were cooled by air (Xu and Zhang, 2002; Perfit et al., 2003; Stevenson et al., 2012).

The final stage, post-cooling, represents the effect of time upon the surface of a flow and is also affected by the presence of water. Devitrification, a common part of the post-cooling stage often seen in volcanic glasses on Earth, is the solid-state process in which glass is transformed into a more structured material (Scott, 1971; Michalski et al., 2006; Horwell et al., 2013; Tornabene et al. 2013; Schipper et al., 2015; Passarella et al., 2017). Altered or secondary minerals, such as smectites and

kaolinites, form due to the presence of water, as the water chemically alters the glass and primary minerals on the lava flow surface into new minerals (Greenberger et al., 2012; Horgan et al., 2017; Yant et al., 2018). On Earth, generally, smectites are best preserved on basalts when the water to rock ratio is low, which can happen in areas with poor drainage or annual dry periods. Typically, basalts will weather into smectite and then into kaolinite when there is a higher water-rock ratio (Jackson and Sherman, 1953; Nesbitt and Young, 1989; Righi and Meunier, 1995).

All four stages produce a final basalt texture, with the fourth stage being on-going, that represents the overall thermal history of the lava as well as containing evidence for lava/water interactions. Since these textures are microscopic, they cannot be studied using the traditional methods of analyzing satellite data, which generally has a spatial resolution too large to study surfaces that closely. So the information about the petrogenesis of the basalt is not available for rocks on other planets. This means that a new method needs to be created to identify these changes in texture using a remote sensing data sets so that glass rich zones can be identified in places, like other planets, where in-depth sample study is not possible.

VNIR, Filling the Gap:

Visible Near Infrared (VNIR) spectroscopy is an important tool used to map the mineralogy of a planet's surface. For our study, we used the Advanced Spaceborne Thermal Emission and Reflection Radiometer (ASTER) to gather VNIR satellite data on our study site, Jordan Craters, and the Terra Spec Halo to gather in-situ VNIR analysis. ASTER data is collected to record the land surface temperature, reflectance, and the elevation of surfaces on Earth. ASTER data sets contain sets of spatial data where the albedo of VNIR can be quantified to see how albedo varies across a flow, allowing for us to identify potential glassy zones. Similar data sets can be collected on Mars using CRISM. The Halo can act as an analog for the equipment on the MSL because the rover's ChemCam spectrometer measures within the range of 350 and 2500nm, which matches the range the Halo measures (Maurice et al., 2012; Black et al., 2016). The major difference between these two instruments is that the MSL samples an area of 20 mrad of 1024×1024 pixels whereas the Halo measures through contact with an area of 1 cm (Maurice et al., 2012; Black et al. 2016).

The light absorbed along this range of wavelengths creates absorption bands which reveal the composition of the surface, e.g. the presence of water will cause absorbance bands at 1400 and 1900 µm. These absorption bands are caused by the two processes; electronic and vibrational. Electronic features are produced by transitions in electron energy, creating features that are broad and found closer to the ultraviolet and visible spectrum (400 to 1000nm). Vibrational features, in contrast, are caused by the vibration of anion groups against the lattice structure of the mineral (Hunt and

Salisbury, 1970). Vibration features are generally found in the near and infrared spectrum, and are sharper than those produced by electronic processes (Hunt and Salisbury, 1970). The presence of these features is used to identify the composition of the surface. Both types of features seen in VNIR are affected by the chemistry and structure of the material and the degree of ordering, which means that in some circumstances absorbance bands of a mineral will not form despite containing that mineral (Arnonson et al., 1966; Adams and McCord, 1969; Minitti et al., 2007; Carli et al. 2015).

The location and depth of an absorbance band in the VNIR spectra can reveal some information about the mineral abundance of the surface, although this is complex because spectra are nonlinearly influenced by the abundance of minerals, particle size, and mineral opacity (e.g., Pieters, 1983; Mustard and Hays, 1997; Poulet and Erard, 2004; Bishop et al., 2014; Roush et al., 2015). This means that correlations between VNIR absorption bands and mineral abundance will be relatively uncertain without the use of end-member spectra to compare with (Poulet and Erard, 2004). Methods like the Modified Gaussian Model have been used to quantify relative mineral abundances while accounting for the effect of grain size, while using end-member spectra found within the VNIR itself (Sunshine and Pieters, 1993; Mustard et al., 1997; Poulet and Erard, 2004). Focusing on the overall albedo of VNIR, however, could allow us to gather more information on mineral and volcanic glass abundance using these same principles.

Albedo is measured on a scale from 0 to 1, with 0 representing a body that absorbs all light and 1 being a body that reflects all light (Coakley, J. A, 2003). Volcanic glass displays an overall reduction, or darkening, in the VNIR's albedo when compared to more crystalline samples (Adams and McCord, 1971; Adams et al., 1974; Bell et al., 1976; McSween and Treiman, 1998; Minitti et al., 2002; McSween et al., 2004; Tompkins and Pieters, 2010; Cannon and Mustard. 2015; Carli et al. 2015; Bishop, 2020). Since water/lava interactions produce petrographic textures that are glassier than air/lava interactions, we hypothesize that water quenched lava can be distinguished from air cooled lava using VNIR because of this effect crystallinity has on overall albedo. We tested this hypothesis using an analog; Jordan Craters, Oregon.

The Analog:

Jordan Craters is a ~3000 years old basaltic lava flow field, with both air and water quenched margins (Otto and Hutchison, 1977)(Figure 1.2). The eastern side of the flow was confined to a stream bed, and quenched by interaction with water, while the western margin was cooled by the air (Otto and Hutchison, 1977). Geochemical analysis indicates that Jordan Craters is an alkaline olivine basalt, with high alumina and low potassium (Hart et al., 1983). Much of the surface of Mars is dominated by similar basaltic compositions and mineralogy, with some samples from the Gale Crater measuring

as basaltic to low potassium basalt (Adams, 1968; Bandfield et al., 2000; Bridges and Warren, 2006; Edwards et al. 2017). Due to the young age and desert location of the eruption, the flow is largely unaltered (Otto and Hutchison, 1977; Hart et al., 1983). Jordan Craters is part of a more complex volcanic system but, on its own, is a relatively simple basalt with no evidence for magma mixing (Hart et al., 1983). Since all lava-water interactions, both solid and liquid water, will produce these glassy textures, we utilized Jordan Craters as the first analog site to identify these interactions. The varying emplacement styles found at Jordan Craters and the lack of alteration allow us to focus solely on the effect that the third stage, emplacement, can have on the albedo of the flow. We will use the data gathered at Jordan Craters to determine if water-lava interactions can be differentiated from air-lava interactions.

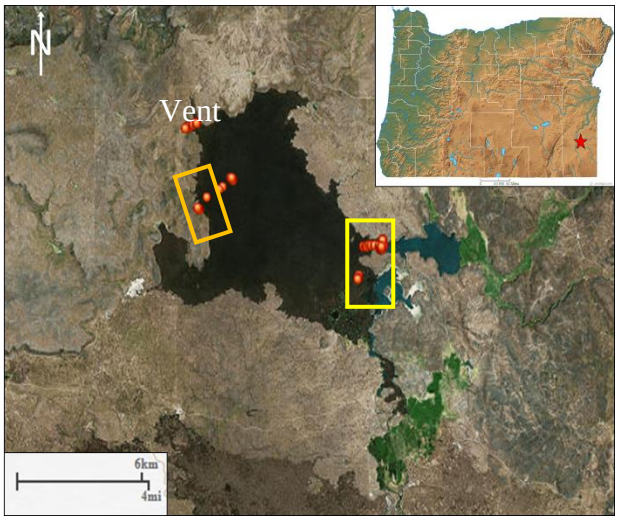

Figure 1.2: A satellite image of Jordan Craters. The sampling sites are represented by red dots with the vent labeled in the Northwest portion of the flow. The water quenched margin is outlined in the yellow box and the sampled air quenched margin is outlined in orange.

Section 2: Methodology

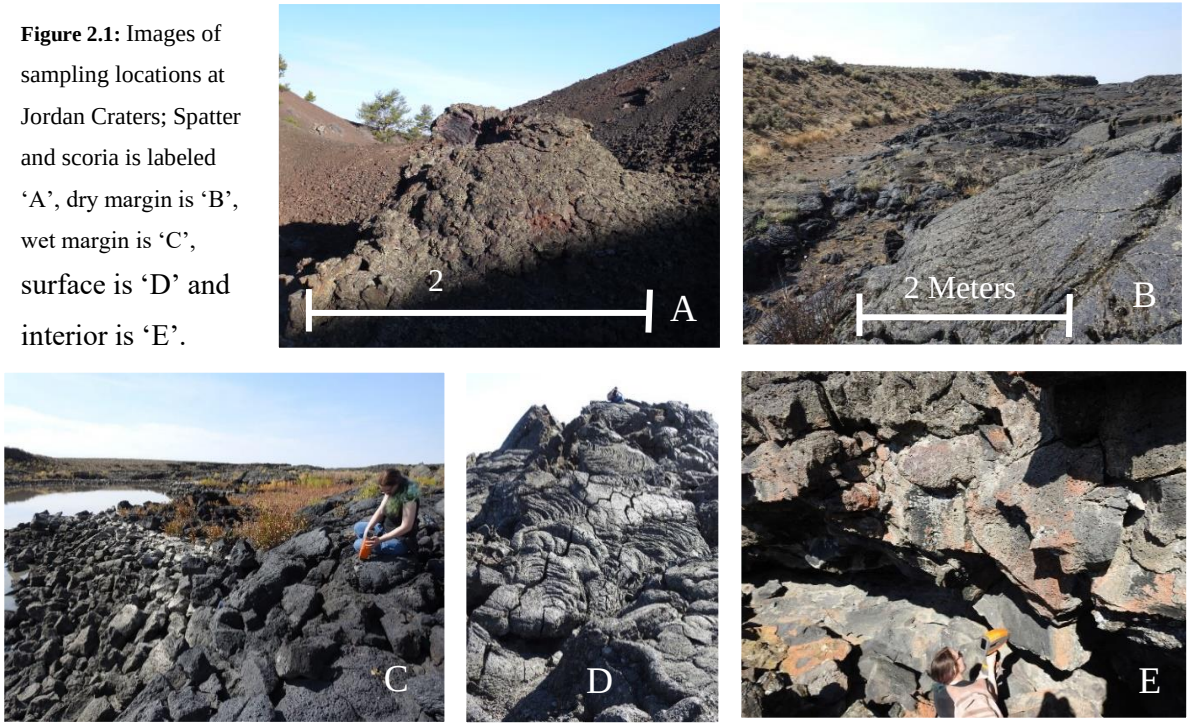

Figure 2.1: Images of sampling locations at Jordan Craters; Spatter and scoria is labeled 'A', dry margin is 'B', wet margin is 'C', surface is 'D' and interior is 'E'.

Field Work:

To examine the textural variability that can develop during emplacement (stage 3), six morphologies were targeted for study. They are, in order from hypothesized fastest to slowest cooling rate; spatter, scoria, wet margin, dry margin, surface, and interior (Figure 2.1). We selected surfaces that were flat, glassy, and visibly free of alteration and lichen to isolate the reflectance of the glass and to control for the effects of the post cooling stage i.e. devitrification and alteration. Jordan Craters had mostly flat, pahoehoe flows, and the other, rougher morphologies like scoria and interior samples were done on the flatter, more vesicle free surfaces, to ensure sampling of all identified morphologies. These samples provide the control for the maximum crystallinity for comparison, since the interior samples would have cooled the slowest. The spatter and scoria samples were meant to represent the most rapidly cooled (and theoretically glassiest) samples. We took samples from both the air quenched and water quenched margins to compare these two environments and determine if they could be differentiated between the vent samples, the spatter and scoria, and the surface samples.

We collected VNIR spectra using an ASD TerraSpec Halo on 95 surfaces and 14 interiors. For most interior samples we looked for interior surfaces that were open to the air, such as those found in collapsed tubes, other interior surfaces, such as those along the margins, sampled had to be broken

since no lichen or dust free surfaces could be found. Breaking open the samples revealed fresh surfaces for the Halo to scan. Each of these surfaces was done in triplicate to account for instrument error, and when measurement was being done the surface was shaded from the sun to control for light pollution. The Halo is a portable contact spectrometer that measures reflected light from between 350 to 2500 nm, with a 6nm band resolution and measures an area with a diameter of 1 cm (Halo Manual, 2015). 15 hand samples were collected at sampling sites to allow for later thin section analysis.

Compositional data was collected using a Bruker Tracer-IV SD portable X-ray fluorescence (pXRF) spectrometer. The pXRF used a 2 W Rh anode X-ray tube and a 10 mm2 Silicon Drift Detector to collect secondary electrons. The pXRF had a voltage of 40 kV with an applied 44 mA probe current. The spot size of the pXRF was 3 mm in diameter which created a total excitation area of ~7 mm2 into the sample. The scanning time was set to 30 seconds per analysis, which was done three times on each surface. The same spot on surfaces was used for both VNIR and pXRF analysis.

Partway through our field expedition the glass plate protecting the pXRF broke, rendering the Bruker unusable for the rest of the trip and resulting in a partial data xrf data set.

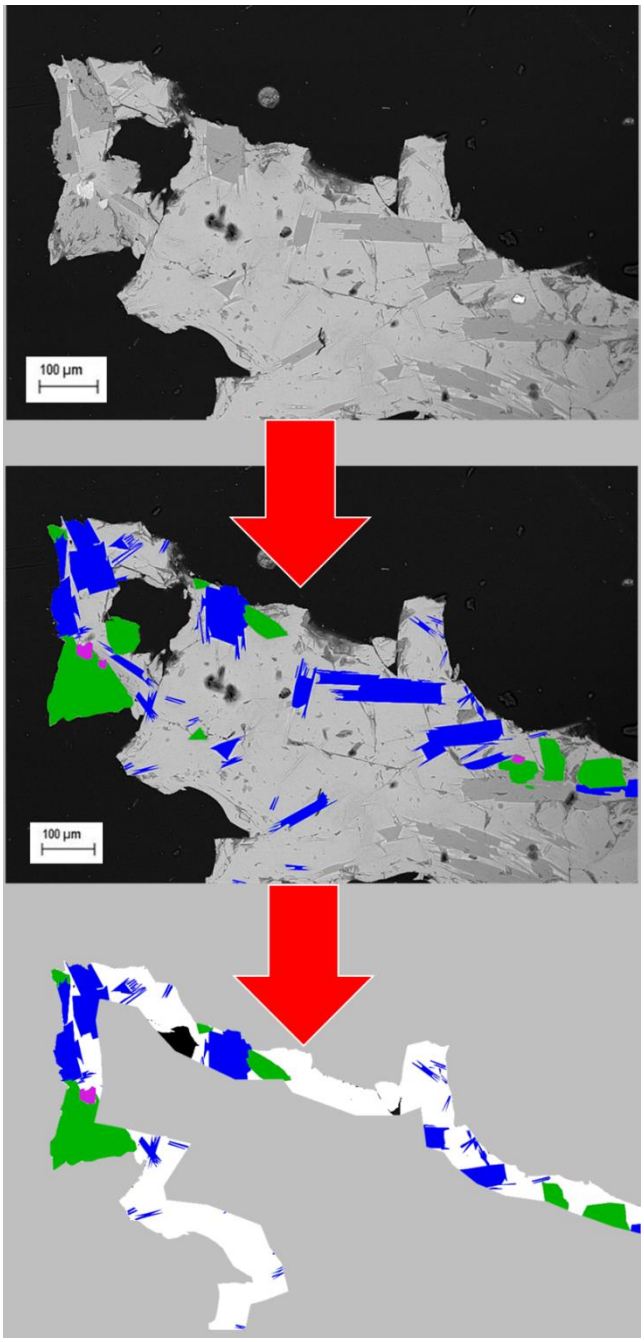

Figure 2.2: Image showing the image analysis process where first modes are identified and outlined (plagioclase in blue, olivine in green, oxides in pink, glass in white, vesicle in black), then a strip 50 microns thick along the rim is cut and the pixel counts of each mode are counted

Lab Work:

The 15 collected hand samples were cut and polished into thin sections. Each thin section had a portion of the outer rim of the samples, these rims were imaged in a Zeiss Supra 35 Variable-Pressure FEG SEM, using Back Scatter Imaging (BSE). Images were taken at a working distance of ~13mm, with an acceleration voltage of 20.00 kV and a magnification of 100x to 300x depending on the complexity of mineralogical texture. We took 10 images per sample, along the entire length of the outer rim which represented ~20 to 40 mm of length depending on the shape of the sample. Elemental maps were produced by scanning the rims using the BSE data for 30 minutes at high resolution to identify where iron, magnesium, aluminum and calcium were present within the image, as these elements are the most relevant to basaltic compositions.

First for each image, the glassy rim was identified and then a strip ~50 microns was cropped using the program software along the rim. This was done to better reflect what the Halo measured in the field, as the Halo can only penetrate ~10 microns into the surface. Based on the magnification of our images, we could only accurately resolve down to the 50-micron strip. Then, we identified six modes; plagioclase, olivine, glass, vesicle, oxide, and devitrification, using GIMP (GIMP 2.10.12) software, an open source photoshopping program (Figure 2.2). Devitrification was identified based on the presence of dendritic or geometric patterns in the glass that had a composition similar to the glass. The mineral phases were identified based on composition and mineral shape. In each image, these modes were isolated and outlined and then the pixel counts for each were recorded. The recorded pixel counts of each image were averaged to produce the overall modal percentages for each sample.

The pixel counts of each mode were then recounted and averaged to compare the overall crystallinity of each sample. The VNIR data was sorted based on morphology, and the albedo values for each were averaged. In this study, the albedo of each of these samples was compared to the calculated modal percentages of the images. Then the overall crystal content (olivine, plagioclase, and oxide) was plotted against the albedo.

Remote Sensing:

ASTER data was collected from the ASTER Volcano Archive (AVA), where remote sensing data for volcanoes is stored and made publicly available. The ASTER data for Jordan Craters was taken during the day on July 10th, 2017 and has a resolution of 15 x 15 meters (Abrams et al., 1999). Using R, first the Digital Numbers (DN), which is how ASTER radiance is recorded, was converted to ‘At-Sensor Radiance’ and then to Top of Atmosphere Reflectance (TOA) to allow for the quantifiable study of albedo. This conversion was done using the following equations (taken from Abrams et al., 1999 and Landsat 7 Users Manual):

$$Radiance = (DN - 1) * ucc$$

$$\rho_{TOA\gamma} = \frac{\pi * L_\gamma * d^2}{ESUN_\sim * cos(\theta_s)}$$

$DN =$ Digital Number
$ucc =$ Unit Conversion Coefficient
$\rho_{TOA\gamma} =$ Top of Atmosphere Reflectance
$L_\gamma =$ Top of Atmosphere Radiance
$d^2 =$ Earth-Sun Distance
$ESUN_\gamma =$ Mean Solar Exoatmospheric Irradiance
$\theta_s =$ Solar Zenith Angle

Each of the three VNIR bands (Band 1, 2 and 3, which measure wavelengths 520-600, 630-690, and 780-860 respectively) were converted to TOA and then the three bands were stacked and averaged in R to get the average albedo for Jordan Craters. The averaged TOA was then mapped to display the variations in albedo across the flow.

Table 2.1 is a summary chart displaying all data collected using these methods. It is ordered based on the time required to complete the analysis for each method.

Data Type	Description
Hand Samples	15 hand samples; 10 BSE images and 5 elemental maps per sample
ASD Halo VNIR	230 flat surfaces measured in situ
Bruker pXRF	50 flat surfaces measured in situ
ASTER	1 Albedo map of entire flow

Table 2.1: A summary of all data collected at Jordan Craters, both in- situ and in the lab. These data sets are ordered from most time consuming to collect to least, with hand sample and image analysis taking weeks to complete and the ASTER map only 1-2 hours.

Section 3: Results

Textures and Observations:

We found four major groups with distinct petrographic textures at Jordan Craters. The first group of textures is simple, with mostly phenocrysts of plagioclase and olivine, and glass (Figure 3.1a). There are some vesicles in these samples but not many, and there is little to no devitrification. There are some microlites of plagioclase and olivine, and they are generally well formed. These samples are mostly seen on glassy surfaces, and they represent the lava that was cooled by air.

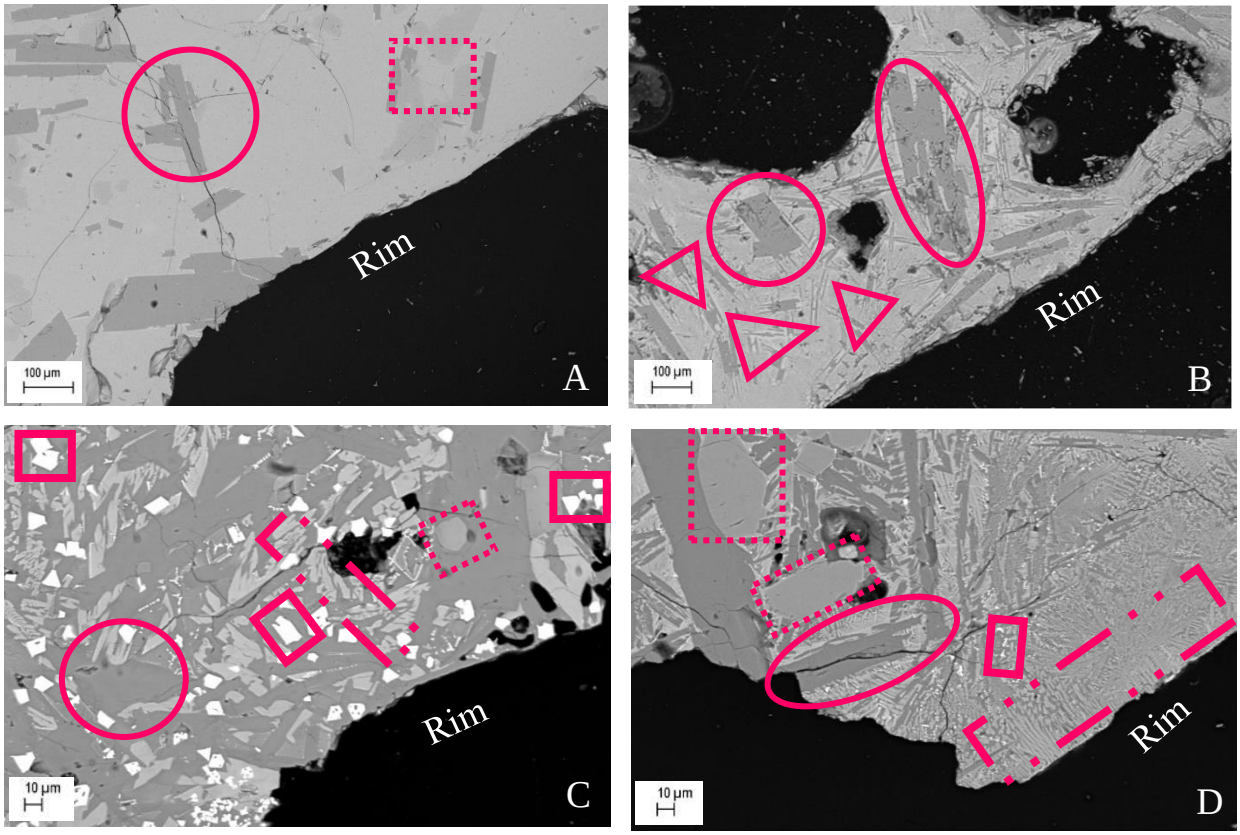

Figure 3.1: BSE SEM images of samples taken from Jordan Craters. Each image displays a unique texture from the flow, with labels. Plagioclase will be outlined in circles, olivine will be outlined in dotted lines, oxides will be outlined in squares, devitrification will be outlined in dashed lines and swallowtail textures will be outlined triangles. The rim of each image is labeled. Sample A is a surface sample, sample B is a water quenched margin, sample C is a spatter sample, and sample D is an interior sample.

The second group is defined by quench textures, while these samples also have phenocrysts of olivine and plagioclase (Figure 3.1b), the plagioclase crystals have swallowtail ends, indicative of rapid quenching. There are also microlites that are thin with sharp tips, also indicative of rapid quenching.

Some of the samples were vesiculated as well. There is some devitrification in the samples, which is most often seen between the swallow tails of the plagioclase crystals.

The third group are surfaces that have a visible glazed texture in hand sample, meaning that the samples were put under heat after cooling. These samples were found in vents and in tubes (Figure 3.1c). The most distinctive characteristic of this group is the presence of well-formed oxide crystals. Some of these samples are red in hand sample, due to the increased amount of Fe-Oxide crystals. The samples also have phenocrysts of olivine and microlites and phenocrysts of plagioclase. There is some devitrification present in the glass of these samples. The final group is defined by large amounts of devitrified glass (Figure 3.1d). These groups, like all previous groups, have phenocrysts and microlites of olivine and plagioclase, but a majority of the measured rim is composed of devitrified glass. The devitrified glass often has a feathery or dendritic texture, which spread out from phenocrysts of plagioclase.

VNIR Findings:

We found absorbance bands at 400nm, 500nm, and 670nm (Figure 3.2). These electronic features represent iron impurities found at Jordan Craters, with the 670nm likely coming from iron within the Mg-rich olivine. We also found vibrational features at 1400nm, 1660nm, 1720nm, 1900nm, 2100nm, 2300nm, and 2400nm (Figure 3.2). The bands at 1400nm and 1900nm are caused by the presence of liquid water within the surface, which we believe was caused by water within the plagioclase crystals. The 2300nm band is caused by molecular water, which we attribute to water within the structure of the olivines. The 2100nm and 2400 nm bands are caused by the vibrations of OH-, the location of this pair of bands is indicative of an Al-rich material with a dioctahedral shape. Thus, we believe that there was the presence of kaolinite dust on some of the surfaces we scanned. The 1660nm and 1720nm bands, which were mostly seen predominately in the spatter and interior morphologies, and are caused by the bending of Al-H-O groups, which also supports the presence of kaolinite dust.

Albedo:

Surface samples had the highest overall albedo and scoria samples had the darkest. The VNIR of the spatter and wet margins were generally flat with little to no visible absorption bands (Figure 3.3,

Table 3.1). Figure 3.3 shows the VNIR spectra of each morphology without offsetting each spectra to show the groupings of albedo. We found that the scoria, spatter, and wet margin morphologies had the lowest albedo, the surface and dry margin morphologies had the next highest albedo and that the interior morphology had the highest albedo overall. We also see that the lowest albedos also contained the least amount of absorbance bands. With spatter being the exception, a majority of bands found on the spatter have been attributed to the presence of dust on measured samples rather than any inherent textural changes (Figure 3.2). Generally we saw that spectra with higher albedos had more distinct bands than darker spectra. When we averaged the albedos for each morphology we found that the 109 measured samples of spatter, scoria, surface, wet margin, dry margin, and interior surfaces had average albedos of ~0.041 ± 0.004, ~0.044 ± 0.007, ~0.056 ± 0.004, ~0.044 ± 0.002, ~0.060 ± 0.002, and ~0.072 ± 0.012 respectively (Table 2.1, Figure 3.4).

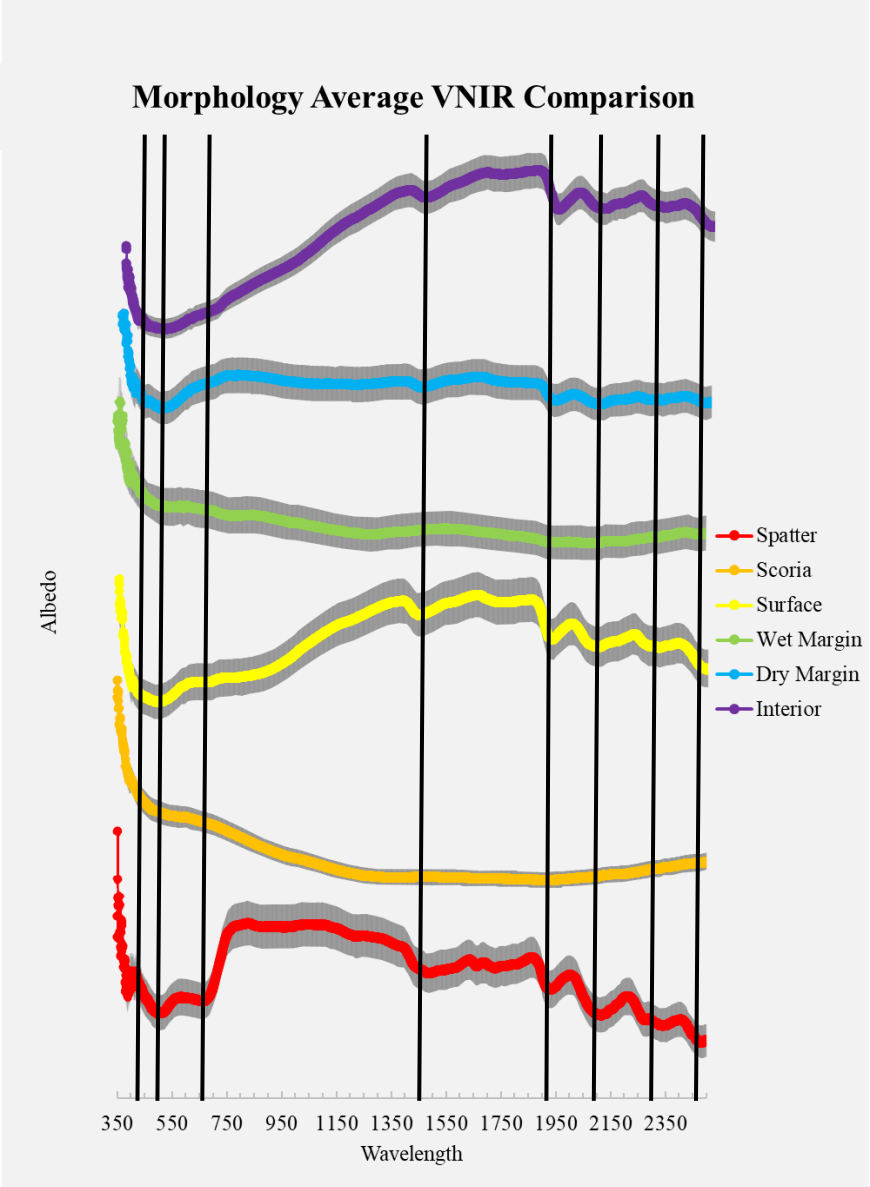

Figure 3.2: VNIR graph showing the average spectra of each morphology. The error of the spectra is shown in gray. The spectrum are offset for clarity, each identified band is shown in black.

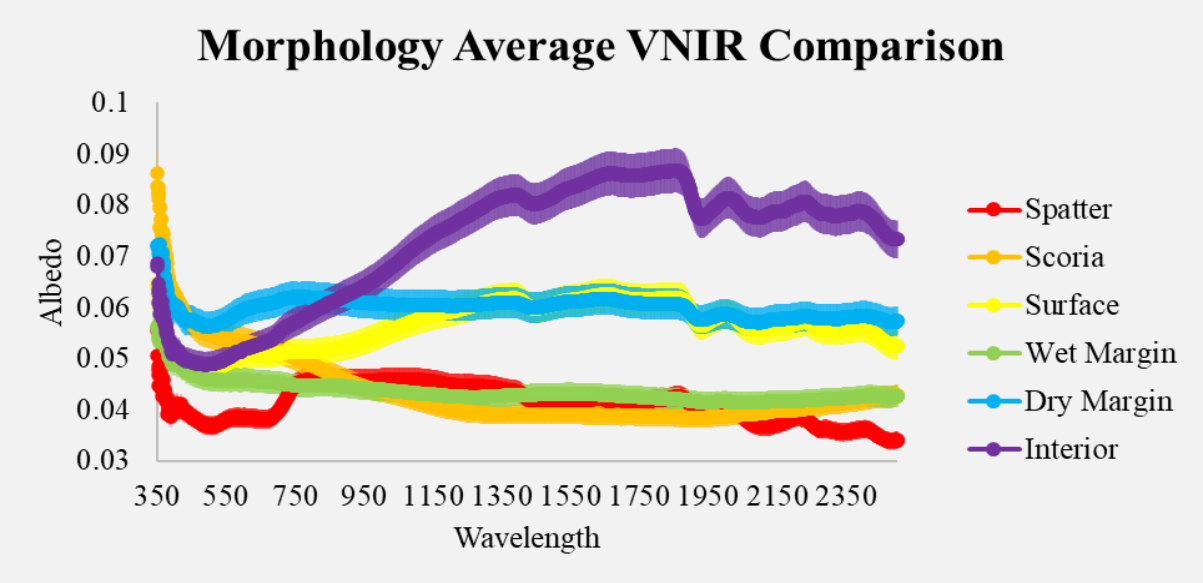

Figure 3.3: A graph showing the average VNIR of each morphology to compare the change in absorbance band size depending on how the sample was quenched or cooled. The spectra are not offset.

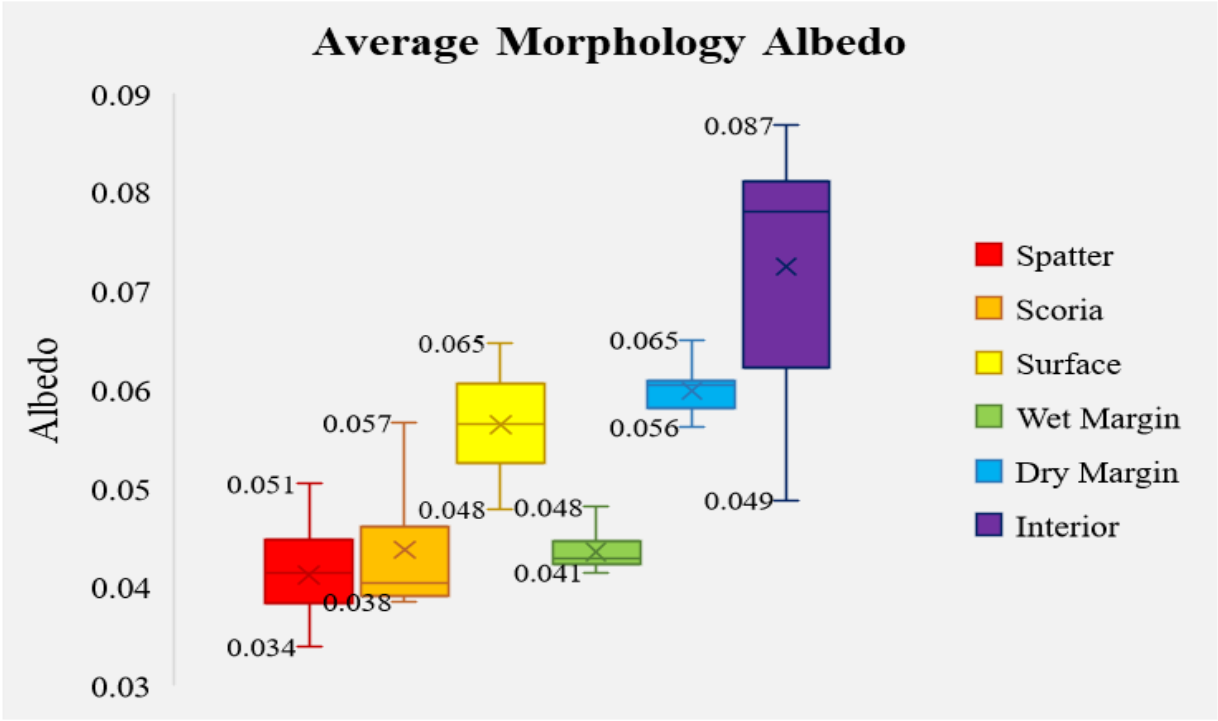

Figure 3.4: Box and Whisker Plot showing the average albedo of each morphology. With Spatter having the lowest measured albedo and the interior surfaces having the highest.

Overall, we see that the dry margin samples were brighter than the wet sample margins. Since the wet margin measurements had little to no bands visible and the dry margin measurements did, we

attribute this change of albedo to changes in crystallinity caused by emplacement style. With the dry margin being more crystalline due to slower cooling when compared to the quenched wet margin.

Modal Percentages of Collected Samples:

The four collected spatter samples had an average glass content of 64%, 10% of which has since devitrified and a crystal percentage of 37%, with plagioclase being the dominant crystal mode at ~28%, and a vesicle percentage of 2% (Figure 3.5, Table 3.1). The two scoria samples had a glass content of 72%, with 9% of the glass being devitrified, the samples had a crystal content of 28%, with plagioclase being the dominant mode at 18% and a vesicle percentage of 7%. The three surface samples' glass content was 75% with no devitrified glass, and a crystal content of 24% with

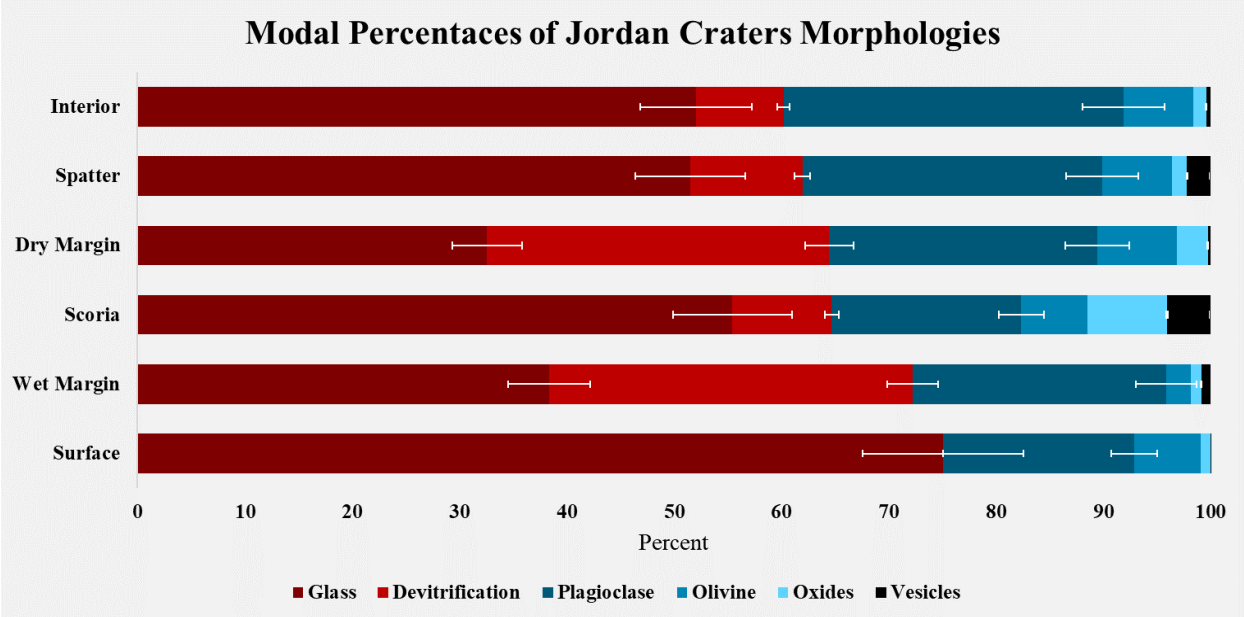

Figure 3.5: A bar graph showing the average modal percentages of the samples taken from Jordan Craters, organized by morphology. Samples are ordered from highest glass content (surface samples) to lowest (interior samples). Glass and devitrified glass are colored in dark red and red to show change on glass content over time, crystal modes are colored in blue to compare overall crystal content to glass content and vesicles are black.

plagioclase being the dominant crystal phase at ~18% and a 1% vesicle mode.

The one wet, or water quenched margin, sample had a glass content of 62%, with 34% of it being devitrified, and a crystal content of 27%, with plagioclase being the dominant crystal mode at ~24% and a vesicle percentage of 1%. Because only one wet margin sample was collected, there is a level of uncertainty about how representative this sample is for the entire wet margin. Further sampling is needed to have a statistical certainty about how the wet margin compares to other morphologies. We found that the two dry, or air quenched, margin samples had a glass content of 60% with ~32% of the

glass having devitrified, and a crystal content of ~33% with the dominant crystal mode being plagioclase at ~25% and a vesicle percentage of 3%. The two interior samples had a glass content of 65% with 8% of the glass being devitrified, and a crystal content of 39% with plagioclase being the dominant crystal mode.

Albedo	Spatter	Scoria	Surface	Wet Margin	Dry Margin	Interior
Minimum	0.034	0.038	0.048	0.041	0.056	0.049
Lower Quartile	0.038	0.039	0.053	0.042	0.058	0.062
Median	0.041	0.040	0.056	0.043	0.060	0.078
Upper Quartile	0.045	0.046	0.061	0.045	0.061	0.081
Maximum	0.051	0.057	0.065	0.048	0.065	0.087
Average	0.041	0.044	0.056	0.044	0.060	0.072
Standard Dev.	0.004	0.007	0.004	0.002	0.002	0.012
Composition						
SiO2	48.52	49.22	49.62	-	-	45.93
Na2O	1.93	2.18	2.35	-	-	1.85
MgO	9.87	8.95	9.15	-	-	9.71
Al2O3	13.24	14.06	15.00	-	-	17.09
P4O6	0.48	0.45	0.71	-	-	0.55
K2O	0.78	0.70	1.53	-	-	0.76
CaO	8.66	9.01	8.33	-	-	9.71
TiO2	2.32	2.19	1.67	-	-	1.83
MnO	0.18	0.19	0.20	-	-	0.20
FeO	14.02	13.06	11.45	-	-	12.36

Table 3.1: Table showing the statistical data for the spectra 114 spectra taken in triplicate at Jordan Craters. This data correlates to the data displayed in Figure 3.2 and is organized based on the designated morphology of the sample. Table also shows average collected values from the pXRF, organized based on morphology. Due to instrumentation failure, no data was gathered for the wet or dry margins

Sample	1	2A	2B	3	4	5	6	7A	7B	8	9	10	11	12	13
Morphology	Scoria	Spatter	Spatter	Spatter	Scoria	Surface	Surface	Interior	Wet Margin	Dry Margin	Dry Margin	Interior	Surface	Dry Margin	Spatter
Glass	71.68	72.01	72.45	35.04	39.21	69.62	73.75	28.17	38.35	25.62	39.53	75.95	81.81	61.90	26.61
St. Dev	8.55	10.49	4.87	17.70	9.20	13.88	9.49	9.86	9.18	10.32	19.40	10.09	8.06	22.22	8.65
Devitrification	0.00	0.00	0.00	22.39	18.52	0.00	0.00	14.04	33.88	30.50	33.31	2.30	0.00	0.00	19.41
St. Dev	0.00	0.00	0.00	9.11	10.09	0.00	0.00	11.19	9.69	17.05	16.59	4.59	0.00	0.00	9.98
Plagioclase	9.71	21.67	16.76	31.40	25.59	22.14	17.61	44.17	23.65	27.75	22.25	19.20	13.80	20.05	41.91
St. Dev	5.04	9.38	4.91	21.40	7.17	10.54	7.47	15.59	11.61	18.04	24.94	9.46	8.99	9.18	13.90
Olivine	7.98	4.71	7.35	8.10	4.39	7.43	7.77	11.62	2.30	12.36	2.47	1.38	3.43	16.43	5.68
St. Dev	7.63	5.92	3.92	12.98	4.77	7.04	6.20	8.31	4.76	21.42	4.29	1.49	5.04	23.66	6.97
Oxides	0.00	0.00	0.03	3.06	8.07	0.00	0.05	0.46	0.86	0.02	0.47	0.35	0.00	0.02	5.80
St. Dev	0.00	0.00	0.07	2.12	4.16	0.00	0.15	0.62	1.25	0.04	0.54	0.63	0.00	0.06	4.40
Vesicle	10.62	1.61	3.40	0.01	4.22	0.81	0.82	1.54	0.95	3.76	1.97	0.82	0.96	1.61	0.58
St. Dev	5.46	1.69	1.26	0.02	4.44	1.15	1.54	1.63	1.30	2.76	4.32	1.01	0.93	2.56	0.97
Albedo	0.04	0.07	0.03	0.03	0.04	0.10	0.05	0.06	0.04	0.06	0.04	0.03	0.04	0.07	0.05
ASTER	0.12	0.11	0.12	0.12	0.12	0.11	0.10	0.12	0.12	0.13	0.13	0.10	0.09	0.12	0.13

Table 3.2: Table showing the modal percentage for each collected sample. These modes include; glass, devitrification, plagioclase, olivine, oxides, and vesicles with the corresponding standard deviations. Along with the modes there is the measured albedo taken from the ASD Halo and the ASTER data calculated from the satellite imagery from the AVA.

ASTER Map:

We created a map of the average of the three VNIR bands of Jordan Craters (Figure 3.6, Table 3.1). The average of the ASTER albedo at the sampling sites for spatter, scoria, surface, wet margin, dry margin, and interior were 0.12 ± 0.00707, 0.12 ± 0, 0.1 ± 0.0082, 0.12 ± 0, 0.127 ± 0.0047, and 0.11 ± 0.01 respectively. The albedo for each morphology was determined by recording the calculated albedo of the sampling sites on the ASTER map and averaging them. Surface samples showed the darkest albedo on ASTER, with a range of 0.09 to 0.11 while margin samples, both dry and wet, had ranges from 0.12 to 0.13. Vent samples had similar albedo levels to margin samples, with a range of 0.11 to 0.13, and were distinguishable solely by looking at the location.

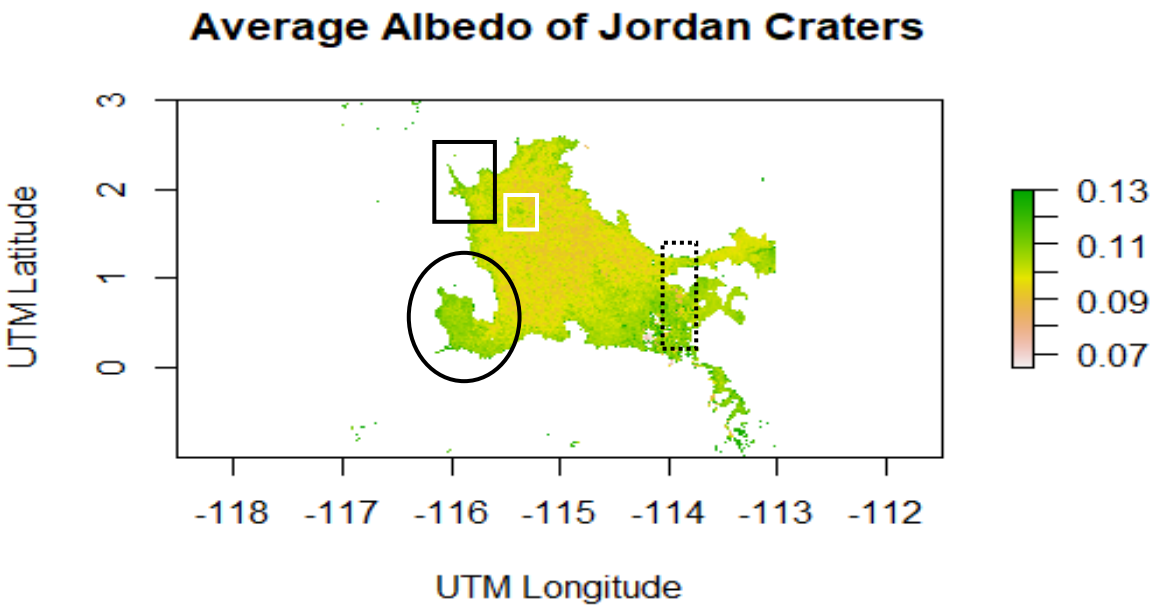

Figure 3.6: An albedo map of Jordan Craters, with the brightest albedo represented in green and the darkest in pink. The vent is outlined in a square, the western dry margin in a circle and the wet margin is outlined in a dotted lines. A bright patch in the center of flow is outlined in white, that represents a collapsed tube. Bright albedo in the south east is due to plant growth.

pXRF Results:

We found that the 7 sampled surfaces at Jordan Craters had a SiO2 content of ~46% to 53% (Figure 3.7, Table 3.1). We were only sampled 7 surfaces due to equipment failure while in the field, leaving this data set incomplete. Overall, the composition of the flow was mafic with a FeO and MgO content of 10-15% and 5- 16%, respectively.

There was a strong negative correlation between CaO and SiO2 with an r value of -0.839 and Al2O3 and SiO2 with an r value of -0.815. There was a weak negative correlation between P4O6 and SiO2 with an r value of -0.343 and TiO2 and SiO2 with and r value of -0.367. There was no correlation between MgO and SiO2, with an r value of -0.262 and FeO and SiO2 with an r value of 0.233. While there was a weak positive correlation between MnO and SiO2 with and r value of 0.406. Both Na2O and SiO2 and K2O had a moderate positive correlation with r values of 0.612 and 0.553 respectively. We believe the variations in composition taken in the field was due to the accuracy of the Bruker. The accuracy of the Bruker is sensitive to the distance, angle, and time that the instrument is held to the surface (Sehlke et al, 2019), with increasing distance and changes in angle causes variations in the results. Figure 3.7 shows how the pXRF results match to lab data collected by Hart et al., which shows that for many of our oxides the variation across the flow is minimal.

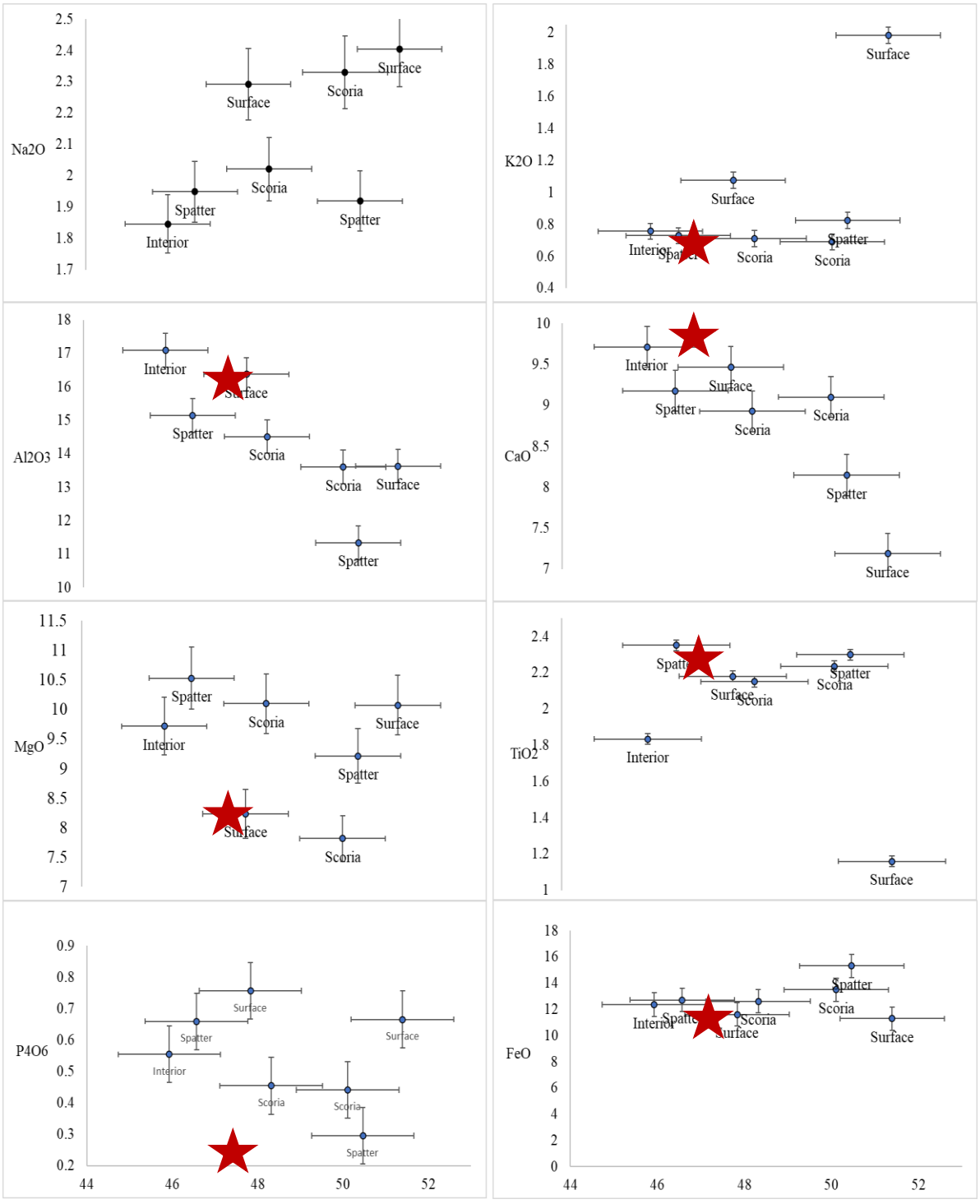

Figure 3.7: Harker Diagrams of geochemical data taken at Jordan Craters. The data shows various trends between oxides and silica and represent the overall change in composition across the flow. Sample morphologies are labeled. The published XRF values from Hart et al., 1983 are represented by red stars.

Section 4: Discussion

In-Situ Findings:

At Jordan Craters we found that overall, when looking at the Halo VNIR data, crystalline samples have much higher albedos and more well-defined absorption bands than glassy samples, The lack of prevalent alteration minerals in the spectra makes sense as this flow is relatively young and we avoided visibly altered surfaces. Water bands could be identified on the more crystalline or devitrified samples, whereas they were not visible on the glassy samples, with only some phenocrysts, since they had almost no absorption bands at all, displaying only flat dark lines (Figure 3.3). This means that the crystallinity of a flow can be broadly differentiated between using only VNIR data. The water quenched margin sample might initially have had glassier textures than air cooled surfaces, however, the presence of devitrification decreased the amount of volcanic glass of the sample during the post-cooling stage, which likely had a brightening effect on the albedo.

The average albedo of the surface samples, the ones with the highest modal percentage of non-devitrified glass, is less than samples that cooled to have less glass, such as the interior samples. Which means that the darkest zones across Jordan Craters end up being the glassy surfaces where there is little to no devitrification and alteration occurring. We theorize that the post-cooling stage has the most effect the measured albedo at Jordan Craters with devitrification being the biggest contributor, to this change. All morphologies had similar amounts of phenocrysts and microlites, but the albedos of these morphologies still varied. The morphologies that had devitrification generally had higher albedos than those that did not. So we believe that the major factor of this change in albedo is due to the presence of devitrification. Based on the amount of measured devitrification, we see that the wet margin sample could originally have had ~72% glass on the surface, which is more measured glass than the glassiest surface samples. This means that before the devitrification occurred the wet margin could have had similar, or even brighter, albedo compared to the surfaces.

At Jordan Craters, we found the most devitrification occurred along the margins, with the wet margin sample having the highest amount at ~33%. Since only one wet margin sample was taken, we cannot be certain if this amount of devitrification is representative for the entire wet margin. We also found that the three dry margin samples had high amounts of devitrification, only ~2% less than the wet margin sample, which is not a significant difference. Our original hypothesis was that the rate of devitrification would be controlled by the presence of water, however there was no visible water along the western (dry) margin, so the high rate of devitrification of both the wet and dry margins could be caused by emplacement location rather than the presence of liquid water. The margins, when

compared to surface or vent samples, would be the portion of the flow most exposed to weathering processes. The brightest samples overall, were the most crystalline, interior samples.

The spectra of partially devitrified samples lie between crystalline interior samples and glassy surface samples, with VNIR signatures that are less distinct and bright than the more crystalline samples. Because the amount of devitrification in a sample has this positive effect on the albedo of the sample, partially devitrified glass on Mars could be identified by comparing the albedo of the sample to more crystalline and more glassy samples, on the same flow, as well as studying the shape and size of the absorption bands.

The existence of partially devitrified glass on Mars has been suggested based on thermal spectral evidence (Torabene et al., 2013; Canon and Mustard, 2015; Farrand et al, 2016). It was found that partially devitrified basaltic glass rinds had VNIR signatures that more closely resemble the signatures found on Mars than pure glass samples, with absorption bands occurring in similar locations (Farrand et al., 2016). Since the rate of devitrification of glass is controlled by the glass viscosity, which is a function of water content and temperature (Friedman and Long, 1984) it is likely that basalts on Mars will have devitrification present, especially those glasses that interacted with water.

The other major factor that did, somewhat, affect Jordan Craters and would likely affect Martian basalts is dust. As seen in Figure 4.1, the samples that had evidence of kaolinite dust on the spectra had much higher albedos but not significantly higher measured crystallinity. These samples had a significantly higher albedo, 0.06 - 0.1, than samples that were glassy, 0.03 - 0.04, while still having similar crystallinity measurements (Figure 4.1).

During our work, any dusts, like kaolinite, that would have been on the surface, were likely washed away during the thin section making process, revealing the unaltered surface below. This meant that the in-situ VNIR samples were brighter, but the crystallinity measurements did not reflect that brightness in the way we hypothesized. The presence of dust is known to increase albedo and so in future work, samples should be cleaned to avoid this effect.

Surface color variations were present at Jordan Craters. Two of our collected spatter samples were red in color due to the presence of Fe-oxide crystals, which were visible in samples that had absorbance bands at 1900 nm. Sample 13 and sample 2A, both spatters with some coloration, had higher albedos than the spatters that were black, with average albedos of 0.046 and 0.068 respectively. The other two spatter samples, 2B and 3, were black in color and had albedos of 0.035 and 0.029. One of the black

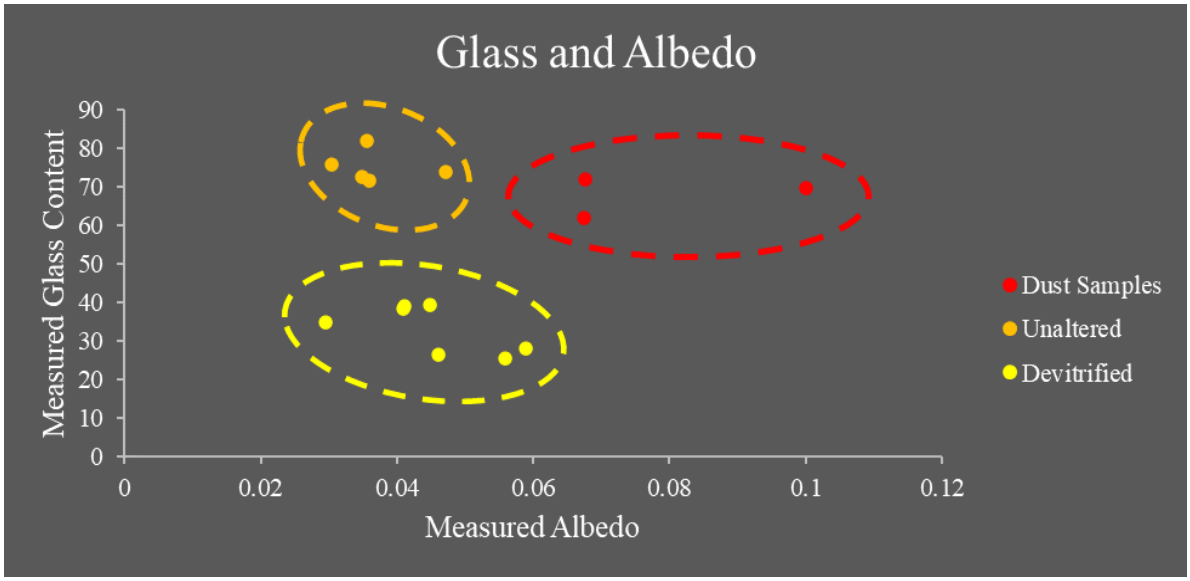

Figure 4.1: Diagram showing the three major groupings of the hand samples found at Jordan Craters, with the measured glass content and it's measured overall albedo. These groupings can be used to roughly estimate the glass content of the surfaces measured using only the Halo.

spatters and one of the colored samples had around ~20% devitrified glass while the other two had no measured devitrified glass. This means that the change in albedo is likely due to this color difference rather than any textural variations caused by devitrification.

Remote Sensing Findings:

The resolution of the ASTER data is 15m x 15m, which allows us to look at the entire flow in a way that we could not using the Halo, but at the cost of losing some spatial resolution. We found that the variations in albedo from the ASTER data matched the changes in crystallinity found in the measured modal percentages of our collected samples. The glassiest areas along the surface, had measured albedos of 0.09 - 0.11 (Table 3.1). There was also an area on the albedo map there were patches on the center of the flow that matched areas of tube collapse (Figure 3.5). Abrupt changes in elevation seem to increase the measured albedo in that area. This is likely due to the angle of the collapsed tube allowing for more light to be reflected back at the sensor than would have been reflected from a flat

surface (Landsat 7 User's Manual). However, understanding how these changes in elevation can affect fully albedo will require more data from flows with more complex topographies.

Using this method of analyzing ASTER data alone we can differentiate broad changes in crystallinity. We can found that the vent and margins had similar albedos but could be differentiated based on shape, with the vent having darker spots of albedo in the center. We cannot yet differentiate between water quenched and air quenched margins. The brightness of both margins on the albedo map is similar enough that we cannot quantify how the margins were quenched, only that they are more crystalline than the glassy surfaces. We could potentially differentiate between these two margins by adding on other remote data sets to help clarify more information about Jordan Craters.

Application on Mars:

Using this method on a rover, which would replicate our in-situ analysis, can provide enough data to differentiate between glassy, dusty, and devitrified basalts. Based on our observations at Jordan Craters we may see a similar effect on Martian basalts, with devitrification and dust increasing albedo. All three of these types of basalts are going to be on Martian flows. Jordan Craters, due to its young age, is most likely less oxidized, devitrified, and dusty than what might be found on a Martian basalt, so more work is needed to fully understand the effect post-cooling can have on albedo (Figure 4.1). This means all four of these 'dusty' basalts can be differentiated using VNIR data collected in-situ, based on the presence of minerals like kaolinite. Differentiating between a devitrified basalt and a crystalline one will be done by comparing overall albedo as well as studying the shape and size of absorption bands. Zones defined by lack of hydrous minerals, flat spectra, and low albedo can be defined as unaltered glassy basalts and can then be graphed in a diagram like Figure 4.1 to give a rough estimate of the glass content.

Using remote sensing data sets on Mars should allow us to broadly identify changes in crystallinity across an entire flow, but without the same level of accuracy as in-situ analysis. These data sets for Mars are produced using instruments like CRISM, which measures a broader range of light than ASTER, with ASTER measuring between 520 and 860nm and CRISM measuring 410 to 3920nm. This broader measured range will likely have its own effect on average albedo that will need to be studied in a future work. Despite this, spatial VNIR data sets will likely be a good first step in identifying zones of lava/water interactions since these data sets can help show relative crystallinity as well as the presence of hydrous minerals on the surface, which could be used to broadly identify glassy, unaltered zones. However, more data sets are needed to confidently differentiate between varying emplacement styles across a flow.

Section 6: Conclusion and Further Study

The goal of this study was to quantify the potential correlation between mineralogical texture and measured albedo of the surface and how this correlation could be used to identify changes in mineral abundances across a lava flow. This correlation could be used to identify lava/water interactions since these interactions produce textures unique from other morphologies on the same flow. Based on our findings at Jordan Craters, identifying lava-water interactions in basalts using this method is possible. Syn-emplacement water-lava interactions had average albedos of ~0.044 and glass percentage of <38. Post-emplacement water interactions had glass modal percentages ranging from 32-58 and albedos of 0.041 to 0.06.

We also found that these changes in albedo were broadly visible using satellite ASTER data, with the margins and vent having brighter albedo than the surface of the flow where the least amount of alteration and devitrification occurred. Our ASTER data was also affected by changes in elevation, which darkened the albedo of a zone without the correlating change in crystallinity. More work needs to be done before we can confidently differentiate between wet and dry margins of flows. If this same method is repeated on many other basalt flows of varying complexity, a refined basalt regime diagram can be created, which can then be used to differentiate between altered, devitrified, and glassy basalts using only VNIR or ASTER data. Once this refined regime diagram is created then this method can be utilized to identify lava/water interactions on the Martian surface.

Literature Cited:

Abrahms, M., Hook, S., and Ramachandran, B., 1999, Aster user handbook, Version 2, NASA/Jet Propulsion Laboratory, Pasadena, CA, at https://asterweb.jpl.nasa.gov/content/03_data/04_Documents/aster_user_guide_v2.pdf.

Adams, J. B., 1986, Lunar and martian surfaces: petrologic significance of absorption bands in the near-infrared. Science. 159(3822):1453-1455. doi:10.1126/science.159.3822.1453

Adams, J. B., and McCord, T. B., 1969, Mars: Interpretation of spectral reflectivity of light and dark regions, J. Geophys. Res., 74(20), 4851– 4856, doi:10.1029/JB074i020p04851.

Adams, J. B., and McCord, T. B., 1971, Optical properties of mineral separates, glass, and anorthositic fragments from Apollo and mare samples. Proceedings of the second lunar science conferences. Vol. 1 pp. 2183-2195.

Adams, J. B., Pieters, C., and McCord T. B., 1974, Orange Glass: Evidence for Regional deposits of pyroclastic origin on the moon. Proceedings of the Fifth Lunar Conference Vol. 1 pp. 171-186

Allen C. C., Gooding J. L., Jercinovic M., Keil K., 1981, Altered basaltic glass: A terrestrial analog to the soil of Mars, Icarus, Volume 45, Issue 2, Pages 347-369, https://doi.org/10.1016/0019-1035(81)90040-3.

Aronson, J. R., Emslie, A. G., & Mclinden, H. G., 1966, Infrared spectra from fine particulate surfaces. Science (New York, N.Y.), 152(3720), 345–346. https://doi.org/10.1126/science.152.3720.345-a

ASD Inc. TerraSpec HALO User Manual: ASD Document, 2015.

Bandfield, J. L., Hamilton, V. E., & Christensen, P. R., 2000, A Global View of Martian Surface Compositions from MGS-TES. Science, 287(5458), 1626–1630. doi: 10.1126/science.287.5458.1626

Bell, P. & Mao, Ho-kwang & Weeks, R., 1976, Optical spectra and electron paramagnetic resonance of lunar and synthetic glasses - A study of the effects of controlled atmosphere, composition, and temperature. Proc. Lunar Sci. Conf. 7. 2543-2559.

Bell, J., 2008, The Martian surface: composition, mineralogy, and physical properties.

Bennett, E., Lissenberg, N., & Cashman, C., 2019, The significance of plagioclase textures in mid-ocean ridge basalt (Gakkel Ridge, Arctic Ocean). Contributions to Mineralogy and Petrology, 174(6), 1–22. https://doi.org/10.1007/s00410-019-1587-1

Bindeman I. N., 2003, Crystal sizes in evolving silicic magma chambers, Geology 31 (4): 367–370. doi: https://doi.org/10.1130/0091-7613(2003)031<0367:CSIESM>2.0.CO;

Bishop, Janice L., 2020, Visible and near-infrared reflectance spectroscopy laboratory spectra of geologic materials, Remote compositional analysis: techniques for understanding spectroscopy, mineralogy, and geochemistry of planetary surfaces, by Janice L. Bishop et al., Cambridge University Press, pp. 68–101.

Bishop J.L., Lane M.D., Dyar M.D., King S.J., Brown A.J., & Swayze G., 2014, Spectral properties of Ca-sulfates: gypsum, bassanite and anhydrite. American Mineralogist, 99, 2105–2115.

Black, S. R., Yingst, A. R., & Hynek, B. M. (2016). Field-Portable VNIR Spectrometry: Applications for Mars Rover Operational Strategies Testing at Terrestrial Analog Sites. Advances in Portable and Handheld Spectroscopy, 31(s9), 29–35. Retrieved from http://ida.lib.uidaho.edu:2048/login?url=https://ida.lib.uidaho.edu:2096/docview/1819908699?accountid=14551

Boreham, F., Cashman, K., Rust, A., & Höskuldsson, Á. (2018). Linking lava flow morphology, water availability and rootless cone formation on the Younger Laxá Lava, NE Iceland. Journal of Volcanology and Geothermal Research, 364, 1–19. doi: 10.1016/j.jvolgeores.2018.08.019

Boston, P.J., Ivanov, M.V., and McKay, C.P., 1992, On the possibility of chemosynthetic ecosystems in subsurface habitats on Mars. Icarus 95:300–308.

Bridges, J., & Warren, P., 2006, The SNC meteorites: basaltic igneous processes on Mars. Journal of the Geological Society, 163(2), 229–251. doi: 10.1144/0016-764904-501.

Brown, A.J., Storrie-Lombardi, M.C., 2006. MR PRISM—A spectral analysis tool for the CRISM. In: Hoover, R.B., Levin, G.V., Rozanov, A.Y. (Eds.), Instruments, Methods, and Missions for Astrobiology IX. In: Proceedings of SPIE, vol. 6309, doi:10.1117/12.677107.

Brown, A.J., Storrie-Lombardi, M.C., 2006, MR PRISM—A spectral analysis tool for the CRISM. In: Hoover, R.B., Levin, G.V., Rozanov, A.Y. (Eds.), Instruments, Methods, and Missions for Astrobiology IX. In: Proceedings of SPIE, vol. 6309, doi:10.1117/12.677107.

Brown, A., Byrne, S., Tornabene, L., & Roush, T. (2008). Louth crater: Evolution of a layered water ice mound. Icarus, 196(2), 433–445. doi: 10.1016/j.icarus.2007.11.023

Brown, A. J., Calvin, W. M., Mcguire, P. C., and Murchie, S. L., 2010, Compact Reconnaissance Imaging Spectrometer for Mars (CRISM) south polar mapping: First Mars year of observations. Journal of Geophysical Research, 115. doi: 10.1029/2009je003333.

Bruno, B. C., Fagents, S. A., Hamilton, C. W., Burr, D. M., and Baloga, S. M. (2006). Identification of volcanic rootless cones, ice mounds, and impact craters on Earth and Mars: Using spatial distribution as a remote sensing tool. Journal of Geophysical Research, 111(E6). doi: 10.1029/2005je002510

Buz, J., and Ehlmann, B. L. (2014). Effects of Grain Size on the Reflectance Spectroscopy of Olivine in the VIS-NIR an the Derivation of Olivine Composition Using Modified Gaussian Modeling . 45th Lunar and Planetary Science Conference. Retrieved from https://www.hou.usra.edu/meetings/lpsc2014/pdf/2810.pdf

Cabane, H., Laporte, D. & Provost, A., 2005, An experimental study of Ostwald ripening of olivine and plagioclase in silicate melts: implications for the growth and size of crystals in magmas. Contrib Mineral Petrol vol 150, pp 37–53, https://doi.org/10.1007/s00410-005-0002-2. Cannon, K. M., & Mustard, J. F. (2015). Preserved glass-rich impactites on Mars. Geology, 43(7), 635–638. doi: 10.1130/g36953.1

Carli, C., Serventi, G., & Sgavetti, M. (2014). VNIR spectral characteristics of terrestrial igneous effusive rocks: mineralogical composition and the influence of texture. Geological Society, London, Special Publications, 401(1), 139–158. doi: 10.1144/sp401.19

Carr MH., 1996, Water on early Mars. Ciba Found Symp., 202:249-267.

Cashman, K. V., 1993, Relationship between plagioclase crystallization and cooling rate in basaltic melts. Contib. Mineral. Petrol. vol 113, pp 126–142.

Cashman K.V., Marsh B.D., 1988, Crystal size distribution (CSD) in rocks and the kinetics and dynamics of crystallization—II: Makaopuhi lava lake. Contrib Mineral Petrol vol 99, pp 292–305.

Chassefière, E., Dartois, E., Herri, J. M., Tian, F., Schmidt, F., Mousis, O. and Lakhlifi, A., 2013, CO2-SO2 clathrate hydrate formation on early Mars, Icarus, vol 223, pp 878 -891, https://doi.org/10.1016/j.icarus.2013.01.001.

Cimarelli, C., Di Traglia, F., and Taddeucci, J., 2010, Basaltic scoria textures from a zoned conduit as precursors to violent Strombolian activity, Geology, 38(5), 439–442. https://doi.org/10.1130/G30720.1

Coakley, J. (2003). Reflectance And Albedo, Surface. Encyclopedia of Atmospheric Sciences, 1914–1923. doi: 10.1016/b0-12-227090-8/00069-5.

Coombs, M. L., Eichelberger, J. C. and Rutherford, M. J., 2002, Experimental and textural constraints on mafic enclave formation in volcanic rocks. Journal of Volcanology and Geothermal Research 119, 125-144.

Cousins, C. R., & Crawford, I. A. (2011). Volcano-Ice Interaction as a Microbial Habitat on Earth and Mars. Astrobiology, 11(7), 695–710. doi: 10.1089/ast.2010.0550

Donato, P., Behrens, H., De Rosa, R., Holtz, F., and Parat, F., 2006, Crystallization conditions in the upper pollara magma chamber, salina island, southern tyrrhenian sea. Mineralogy and Petrology, 86(1-2), 89-108. doi:http://ida.lib.uidaho.edu:2153/10.1007/s00710-005-0105-5

Dyar, M., and Schaefer, M. W., 2004, Mössbauer spectroscopy on the surface of Mars: constraints and expectations. Earth and Planetary Science Letters, 218(3-4), 243–259. doi: 10.1016/s0012-821x(03)00689-7

Edwards, P. H., Bridges, J. C., Wiens, R., Anderson, R., Dyar, D., Fisk, M., … Hutchinson, I. (2017). Basalt-trachybasalt samples in Gale Crater, Mars. Meteoritics & Planetary Science. doi: 10.1111/maps.12953

Ehlmann, B. L., Mustard, J. F., Murchie, S. L., Bibring, J.-P., Meunier, A., Fraeman, A. A., & Langevin, Y. (2011). Subsurface water and clay mineral formation during the early history of Mars. Nature, 479(7371), 53–60. doi: 10.1038/nature10582

Fagents, S. A., & Thordarson, T. (2007). Rootless volcanic cones in Iceland and on Mars. The Geology of Mars, 151–177. doi: 10.1017/cbo9780511536014.007

Farmer, J.D., 1996, Hydrothermal systems on Mars: an assessment of present evidence. In Evolution of Hydrothermal Ecosystems on Earth (and Mars?), Ciba Foundation Symposium 202, edited by G.R. Bock and J.A.

Farrand, W. H., Rogers, A. D., Wright, S. P., & Glotch, T. D. (2016). Partially Devitrified Glass as a Component of the Martian Surface Layer: Thermal Infrared Evidence. 47th Lunar and Planetary Conference. Retrieved from https://www.hou.usra.edu/meetings/lpsc2016/pdf/1956.pdf

Farrand, W. H., Johnson, J. R., Rice, M. S., Wang, A., & Bell, J. F. (2016). VNIR multispectral observations of aqueous alteration materials by the Pancams on the Spirit and Opportunity Mars Exploration Rovers. American Mineralogist, 101(9), 2005–2019. doi: 10.2138/am-2016-5627

Fisk, M. R., & Giovannoni, S. J. (1999). Sources of nutrients and energy for a deep biosphere on Mars. Journal of Geophysical Research: Planets, 104(E5), 11805–11815. doi: 10.1029/1999je900010

Friedman, I., & Long, W. (1984). Volcanic glasses, their origins and alteration processes. Journal of Non-Crystalline Solids, 67(1), 127–133. https://doi.org/10.1016/0022-3093(84)90144-3

Ginibre, C., Wörner, G., Kronz, A., 2002, Minor- and trace-element zoning in plagioclase: implications for magma chamber processes at Parinacota volcano, northern Chile. Contrib Mineral Petrol 143:300–315. https://doi.org/10.1007/s00410-002-0351-z

Gulick, V.C., 1998, Magmatic intrusions and a hydrothermal origin for fluvial valleys on Mars. J Geophys Res 103:19365– 19387.

Greeley R., and Fagents S. A., 2001, Icelandic pseudocraters as analogs to come volcanic cones on Mars, J. Geophys. Res., 106, pp. 20, 527-20, 546.

Hamilton C. W., Fagents S.A., Thordarson T.H., 2011, Lava-ground ice interaction in Elysium Planitia, Mars: Geomorphological and geospatial analysis of the Tartarus Colles cone groups J. Geophys. Res., 116, Article E03004

Hart, W. K., & Mertzman, S. A. (1983). Late Cenozoic volcanic stratigraphy of the Jordan Valley area, southeastern Oregon . Oregon Geology, 45(2), 15–19. Retrieved from https://www.oregongeology.org/pubs/og/OGv45n02.pdf

Haskin, L., Wang, Al., Jolliff, B., McSween, H., Clark, B., Des M. D., McLennan, S., Tosca, N., Hurowitz, J., Farmer, J., Yen, A., Squyres, S., Arvidson, R., Klingelhoefer, G., Schröder, C., & De Souza, P., Ming, D., Gellert, R., and Soderblom, L., 2005, Water alteration of rocks and soils on Mars at the Spirit rover site in Gusev crater. Nature. 436. 66-9. 10.1038/nature03640.

Hecker, C., Meijde, M. V. D., & Meer, F. D. V. D., 2010, Thermal infrared spectroscopy on feldspars — Successes, limitations and their implications for remote sensing. Earth-Science Reviews, 103(1-2), 60–70. doi: 10.1016/j.earscirev.2010.07.005

Hon, K., Kauahikaua, J., Denlinger, R., & Mackay, K., 1994, Emplacement and inflation of pahoehoe sheet flows: observations and measurements of active lava flows on Kilauea Volcano, Hawaii. The Geological Society of America Bulletin, 106(3), 351–370. https://doi.org/10.1130/0016-7606(1994)106<0351:EAIOPS>2.3.CO;2

Horgan, B. H. N., Smith, R. J., Cloutis, E. A., Mann, P., and Christensen, P. R., 2017, Acidic weathering of basalt and basaltic glass: 1. Near-infrared spectra, thermal infrared spectra, and implications for Mars, J. Geophys. Res. Planets, 122, 172– 202, doi:10.1002/2016JE005111.

Horwell, C., Williamson, J., Llewellin, B., Damby, E., & Blond, W., 2013, The nature and formation of cristobalite at the Soufrière Hills volcano, Montserrat: implications for the petrology and stability of silicic lava domes. Bulletin of Volcanology, 75(3), 1–19. https://doi.org/10.1007/s00445-013-0696-3

Howard, K.T., et al., 2013, Biomass preservation in impact melt ejecta: Nature Geoscience, v. 6, p. 1018–1022, doi:10.1038/ngeo1996.

Hovius, N., Lea-Cox, A., and Turowski, J.M., 2008, Recent volcano-ice interaction and outburst flooding in a Mars polar cap re-entrant. Icarus 197:24–38.

Hunt, G. R., & Salisbury, J. W. (1970). Visible and Near-Infrared Spectra of Minerals and Rocks: I Silicate Minerals. Modern Geology, 1, 283-300.

Jackson, M. L., and Sherman G. D., 1953, Chemical weathering of minerals in soils, Adv. Agron., 5, 219–318, doi:10.1016/S0065-2113(08)60231-X.

Jafri, S., & Charan, H., 1992, Quench textures in pillow basalt from the Andaman-Nicobar Islands, Bay of Bengal, India. Proceedings of the Indian Academy of Sciences - Earth and Planetary Sciences, 101(1), 99–107. https://doi.org/10.1007/BF02839176

Jakobsson, S., and Gudmundsson, M., 2008, Subglacial and intraglacial volcanic formations in Iceland. Jökull. 58.

Keszthelyi, L., 1995, A preliminary thermal budget for lava tubes on the Earth and planets, J. Geophys. Res., 100(B10), 20411– 20420, doi:10.1029/95JB01965.]

Landsat 7 Science Data Users Handbook: https://landsat.gsfc.nasa.gov/wp-content/uploads/2016/08/Landsat7_Handbook.pdf.

Lofgren G., 1974, An experimental study of plagioclase crystal morphology: isothermal crystallization. Am J Sci 274:243–273

Navarro-Gonzalez, R., Navarro, K. F., Rosa, J. D. L., Iniguez, E., Molina, P., Miranda, L. D., … Mckay, C. P., 2006, The limitations on organic detection in Mars-like soils by thermal volatilization-gas chromatography-MS and their implications for the Viking results. Proceedings of the National Academy of Sciences, 103(44), 16089–16094. doi: 10.1073/pnas.0604210103

Nelson S.T., Montana A., 1992, Sieve-textured plagioclase in volcanic rocks produced by rapid decompression. Am Mineral 77:1242–1249

Nesbitt, H. W., and G. M. Young, 1989, Formation and diagenesis of weathering profiles, J. Geol., 97(2), 129–147, doi:10.1086/629290.

Martin, W., Baross, J., Kelley, D., and Russell, M., 2008,. Hydrothermal vents and the origin of life. Nature Rev. Microbiol.. 29. 1-10.

Maurice, S., Wiens, R.C., Saccoccio, M. et al., 2012, The ChemCam Instrument Suite on the Mars Science Laboratory (MSL) Rover: Science Objectives and Mast Unit Description. Space Sci Rev 170, 95–166, https://doi.org/10.1007/s11214-012-9912-2

Mckay, C. and Stoker, C., 1989, The early environment and its evolution on Mars: Implication for life. Reviews of Geophysics. 27. 10.1029/RG027i002p00189.

McKay, C., and Davis, W., 1991, Duration of liquid water habitats on early Mars. Icarus. 90. 214-221. 10.1016/0019-1035(91)90102-Y.

McKay, C., Mancinelli, R., Stoker, C., and Wharton R. A., 1992, The possibility of life on Mars during a water-rich past. SEE A93-27852; In: Mars (A93-27852 09-91); p. p. 1234-1245.

Mckay, C. P., Friedman, E. I., Wharton, R. A., & Davies, W. L. (1992). History of water on Mars: A biological perspective. Advances in Space Research, 12(4), 231–238. doi: 10.1016/0273-1177(92)90177-y

McSween H.Y.Jr. and Treiman A.H., 1998, Martian Samples, Chapter VI in Planetary Materials (J.J. Papike ed.), Reviews in Mineralogy, vol. 36, Mineralogical Society America.

McSween, H. Y., Arvidson, R. E., Bell, J. F., 3rd, Blaney, D., Cabrol, N. A., Christensen, P. R., Clark, B. C., Crisp, J. A., Crumpler, L. S., Des Marais, D. J., Farmer, J. D., Gellert, R., Ghosh, A., Gorevan, S., Graff, T., Grant, J., Haskin, L. A., Herkenhoff, K. E., Johnson, J. R., Jolliff, B. L., … Zipfel, J. (2004). Basaltic rocks analyzed by the Spirit Rover in Gusev Crater. Science (New York, N.Y.), 305(5685), 842–845. https://doi.org/10.1126/science.1099851

Michalski, J., Kraft, M., Sharp, T., & Christensen, P. (2006). Effects of chemical weathering on infrared spectra of Columbia River Basalt and spectral interpretations of martian alteration. Earth and Planetary Science Letters, 248(3-4), 822–829. doi: 10.1016/j.epsl.2006.06.034

Minitti, M. E., Mustard, J. F., and Rutherford, M. J., (2002), Effects of glass content and oxidation on the spectra of SNC-like basalts: Applications to Mars remote sensing, J. Geophys. Res., 107(E5), doi:10.1029/2001JE001518.

Minitti, M. E., Weitz, C. M., Lane, M. D., and Bishop, J. L. (2007), Morphology, chemistry, and spectral properties of Hawaiian rock coatings and implications for Mars, J. Geophys. Res., 112, E05015, doi:10.1029/2006JE002839.

Morris, R. & Graff, T. & Ming, D. & Bell, & le, Lynn & Mertzman, Stanley & Christensen, P.. (2004). Palagonitic Mars: A Basalt Centric View of Surface Composition and Aqueous Alteration.

Murchie, S.L. & Seelos, F.P. & Hash, C.D. & Humm, D.C. & Malaret, E. & McGovern, J.A. & Seelos, K.D. & Buczkowski, D.L. & Morgan, Frank & Barnouin, O. & Nair, Hari & Taylor, H.W. & Patterson, G.W. & Harvel, C.A. & Mustard, John & Arvidson, Raymond & McGuire,

Mustard J.F. & Hays J.E., (1997), Effects of hyperfine particles on reflectance spectra from 0.3 to 25 μm. Icarus, 125, 145–163.

Mustard, J. F., Murchie, S., Erard, S., and Sunshine, J. (1997), In situ compositions of Martian volcanics: Implications for the mantle, J. Geophys. Res., 102(E11), 25605– 25615, doi:10.1029/97JE02354.

Otto, B. R., & Hutchison, D. A. (1977). The Geology of Jordan Craters, Malheur County, Oregon. The Ore Bin, 39(8), 128–139. Retrieved from https://www.oregongeology.org/pubs/og/OBv39n08.pdf

Pan, Y., Batiza, R., (2003), Magmatic processes under mid-ocean ridges: a detailed mineralogic study of lavas from East Pacific rise 9°30′N, 10°30′N, and 11°20′N. Geochem Geophys Geosyst

Passarella, M., Mountain, B. W., & Seward, T. M., (2017), Experimental Simulations of Basalt-fluid Interaction at Supercritical Hydrothermal Condition (400°C – 500bar). Procedia Earth and Planetary Science, 17, 770–773. https://doi.org/10.1016/j.proeps.2017.01.022

Patrick & Smith, M.D. & Wolff, M. & Titus, Timothy. (2009). The CRISM Investigation and Data Set from the Mars Reconnaissance Orbiter's Primary Science Phase. Journal of Geophysical Research. 114.

Payne, M.C. and Farmer, J.D., (2001), Volcano-ice interactions and the exploration for extant martian life [abstract #P22B-0549]. In 2001 AGU Fall Meeting, American Geophysical Union, Washington DC.

Perfit, M. R., Cann, J. R., Fornari, D. J., and Engels, J., (2003), Interaction of sea water and lava during submarine eruptions at mid-ocean ridges. Nature, 426(6962), 62-5. doi:http://ida.lib.uidaho.edu:2153/10.1038/nature02032

Pichavant, M., Martel, C., Bourdier, J. L., and Scaillet, B., (2002), Physical conditions, structure and dynamics of a zoned magma chamber : Mount Pelée (Martinique, Lesser Antilles arc).. Journal of Geophysical Research : Solid Earth, American Geophysical Union, 107, pp.101029-101055. ff10.1029/2001JB000315ff. ffhal-00072954f

Pieters C.M., (1983), Strength of mineral absorption features in the transmitted component of near-infrared reflected light: First results from RELAB. Journal of Geophysical Research, 88, 9534–9544.

Poulet, F., and Erard, S. (2004), Nonlinear spectral mixing: Quantitative analysis of laboratory mineral mixtures, J. Geophys. Res., 109, E02009, doi:10.1029/2003JE002179.

Postawko, S. & Kuhn, W.R., (1986), Effect of the greenhouse gases (CO2, H2O, S2O) on martian paleoclimate. Journal of Geophysical Research. 91.

Pupier, E., Duchene, S., & Toplis, M. J. (2007). Experimental quantification of plagioclase crystal size distribution during cooling of a basaltic liquid. Contributions to Mineralogy and Petrology, 155(5), 555–570. doi: 10.1007/s00410-007-0258-9

Righi, D., and Meunier, A., (1995), Origin of clays by rock weathering, in Origin and Mineralogy of Clays, pp. 43–161, Springer, Berlin.

Roush T.L., Bishop J.L., Brown A.J., Blake D.F., & Bristow T.F., (2015), Laboratory reflectance spectra of clay minerals mixed with Mars analog materials: Toward enabling quantitative clay abundances from Mars spectra. Icarus, 258, 454–466

Sætre, C., Hellevang, H., Riu, L., Dypvik, H., Pilorget, C., Poulet, F. and Werner, S.C., (2019), Experimental hydrothermal alteration of basaltic glass with relevance to Mars. Meteorit Planet Sci, 54: 357-378. doi:10.1111/maps.13214

Salisbury, M. J., Bohrson, W. A., Clynne, M. A., Ramos, F. C., & Hoskin, P., (2008), Multiple Plagioclase Crystal Populations Identified by Crystal Size Distribution and in situ Chemical Data: Implications for Timescales of Magma Chamber Processes Associated with the 1915 Eruption of Lassen Peak, CA. Journal of Petrology, 49(10), 1755–1780. https://doi.org/10.1093/petrology/egn045

Sato, H. (1995), Textural difference between pahoehoe and aa lavas of Izu-Oshima volcano, Japan — an experimental study on population density of plagioclase, Journal of Volcanology and Geothermal Research, v. 66, p. 101-113, https://doi.org/10.1016/0377-0273(94)00055-L.

Schipper, C., Castro, I., Tuffen, J., Wadsworth, M., Chappell, H., Pantoja, F., … Le Ru, D., (2015), Cristobalite in the 2011–2012 Cordón Caulle eruption (Chile). Bulletin of Volcanology, 77(5), 1–19. https://doi.org/10.1007/s00445-015-0925-z

Schultz, P.H., Harris, R.S., Clemett, S.J., ThomasKeprta, K.L., and Zárate, M., (2014), Preserved flora and organics in impact melt breccias: Geology, v. 42, p. 515–518, doi:10.1130/G35343.1

Scott, R. B., (1971), Alkali Exchange during Devitrification and Hydration of Glasses in Ignimbrite Cooling Units. The Journal of Geology, 79(1), 100–110. https://doi.org/10.1086/627591

Sehlke, A., Mirmalek, Z., Burtt, D., Haberle, C. W., Santiago-Materese, D., Nawotniak, S. E. K., … Lim, D. S. (2019). Requirements for Portable Instrument Suites during Human Scientific Exploration of Mars. Astrobiology, 19(3), 401–425. doi: 10.1089/ast.2018.1841

Slovenec, D., Lugovic, B., & Slovenec, D., (2012), Secondary mineral paragenesis in the mafic extrusive rocks from the Mt. Medvednica ophiolite melange (Croatia)/Sekundarne mineralne parageneze u mafitnim ekstruzivnim stijenama iz ofiolitnog melanza Medvednice (Hrvatska). Rudarsko-Geolosko-Naftni Zbornik, 25, 33+. Retrieved from https://ida.lib.uidaho.edu:7215/apps/doc/A360863724/AONE?u=mosc00780&sid=AONE&xid=6087c8bc

Stevenson, J. A., Mitchell, N. C., Mochrie, F., Cassidy, M., & Pinkerton, H., (2012), Lava penetrating water: The different behaviours of pahoehoe and 'a'a at the nesjahraun, [THORN]ingvellir, iceland. Bulletin of Volcanology, 74(1), 33-46. doi:http://ida.lib.uidaho.edu:2153/10.1007/s00445-011-0480-1

Sun, H., Zhong, D., Zhan, W., & Qiu, N., (2019), Reservoir characteristics in the Cretaceous volcanic rocks of Songliao Basin, China: A case of dynamics and evolution of the volcano-porosity and diagenesis. Energy Exploration & Exploitation, 37(2), 607–625. https://doi.org/10.1177/0144598718812546

Sunshine, J. M., and Pieters, C. M. (1993), Estimating modal abundances from the spectra of natural and laboratory pyroxene mixtures using the modified Gaussian model, J. Geophys. Res., 98(E5), 9075– 9087, doi:10.1029/93JE00677.

Szramek, L., Gardner, J. E. & Larsen, J., (2006), Degassing and microlite crystallization of basaltic andesite magma erupting at Arenal Volcano, Costa Rica. J. Volcanol. Geotherm. Res. 157, 182–201.

Szramek L., Gardner, J. E., Hort, M., (2010) Cooling-induced crystallization of microlite crystals in two basaltic pumice clasts. American Mineralogist ; 95 (4): 503–509. doi: https://doi.org/10.2138/am.2010.3270

Tompkins, S. and Pieters, C. M., (2010), Spectral characteristics of lunar impact melts and inferred mineralogy. Meteoritics & Planetary Science, 45: 1152-1169. doi:10.1111/j.1945-5100.2010.01074.x

Tornabene, L. L., Osinski, G. R., Mcewen, A. S., Wray, J. J., Craig, M. A., Sapers, H. M., & Christensen, P. R. (2013). An impact origin for hydrated silicates on Mars: A synthesis. Journal of Geophysical Research: Planets, 118(5), 994–1012. doi: 10.1002/jgre.20082

Ustunisik, G., Kilinc, A., Nielsen, R. L., (2014), New insights into the processes controlling compositional zoning in plagioclase. Lithos 200–201:80–93. https://doi.org/10.1016/j.lithos.2014.03.021

Valentine, G. A., Krier, D. J., Perry, F. V., and Heiken, G., (2007), Eruptive and geomorphic processes at Lathrop Wells scoria cone volcano: Journal of Volcanology and Geothermal Research, v. 161, p. 57–80, doi: 10.1016/j.jvolgeores.2006.11.003

Wall, K. T., Rowe, M. C., Ellis, B. S., Schmidt, M. E., & Eccles, J. D. (2014). Determining volcanic eruption styles on Earth and Mars from crystallinity measurements. Nature Communications, 5(1). doi: 10.1038/ncomms6090

Warner, N. H. and Farmer, J. D., (2010), Subglacial hydrothermal alteration minerals in Jökulhlaup deposits of Southern Iceland, with implications for detecting past or present habitable environments on Mars. Astrobiology. 10(5):523-547. doi:10.1089/ast.2009.0425

Xu, Z., & Zhang, Y., (2002), Quench rates in air, water, and liquid nitrogen, and inference of temperature in volcanic eruption columns. Earth and Planetary Science Letters, 200(3-4), 315–330. doi: 10.1016/s0012-821x(02)00656-8

Yant, M., Young, K. E., Rogers, A. D., McAdam, A. C., Bleacher, J. E., Bishop, J. L., & Mertzman, S. A., (2018), Visible, near-infrared, and mid-infrared spectral characterization of Hawaiian fumarolic alteration near Kilaueas December 1974 flow: Implications for spectral discrimination of alteration environments on Mars. American Mineralogist, 103(1), 11–25. doi: 10.2138/am-2018-6116

Young, L. A., Aiken, E., Lee, P. and Briggs, G., (2005), "Mars rotorcraft: possibilities, limitations, and implications for human/robotic exploration," 2005 IEEE Aerospace Conference, Big Sky, MT, pp. 300-318, doi: 10.1109/AERO.2005.1559324